Advances in Nano Research, *Vol. 18, No. 4 (2025) 321-335*
https://doi.org/10.12989/anr.2025.18.4.321

Dynamic stability and vibration responses of a volleyball game ball

Zhao Daichang[1], Li Aiyun[2], Song Zhiqiang*[1], Mostafa Habibi[3,4,5], Ibrahim Albaijan[6] and Lian Wong[5]

[1]*College of Physical Education, Shandong Sport University, 276826, China*
[2]*College of Sports and Health, Shandong Sport University, 276826, China*
[3]*Universidad UTE, Facultad de Arquitectura y Urbanismo, Calle Rumipamba S/N y Bourgeois, Quito 170147, Ecuador*
[4]*Department of Biomaterials, Saveetha Dental College and Hospital, Saveetha Institute of Medical and Technical Sciences, Chennai 600 077, India*
[5]*Institute of Research and Development, Duy Tan University, Da Nang 550000, Viet Nam*
[6]*Mechanical Engineering Department, College of Engineering at Al Kharj, Prince Sattam Bin Abdulaziz University, Al Kharj 16273, Saudi Arabia*

(*Received September 19, 2021, Revised January 3, 2025, Accepted January 16, 2025*)

Abstract. This study investigates the vibrational response of a graphene oxide-reinforced volleyball under impact loading, aiming to enhance its dynamic stability. Employing Hamilton's principle and spherical shell coordinates, we derive the governing equations for the ball's motion under internal loading. These equations are solved using the generalized differential quadrature (GDQ) method and analytical techniques to analyze the vibrational modes. The results demonstrate a significant correlation between the ball's radius and its dynamic stability, with variations in radius substantially affecting vibrational characteristics. Notably, we find that increased ball mass, independent of size, contributes to enhanced stability upon ground impact. This observation suggests that heavier balls exhibit improved resistance to deformation and vibration, leading to more predictable trajectories. The findings provide a quantitative basis for optimizing volleyball design by elucidating the interplay between material reinforcement, geometry, and impact dynamics, thereby facilitating the development of volleyballs with improved stability and performance.
Keywords: ball's radius; GDQM; stability; vibration; volleyball game ball

1. Introduction

Tools in the sport games are essential part of most games. By tools, we mean clothing, balls, shoes and any other structures and devices used by athletes. It is obvious that quality and characteristics of the tools could make great influence on the performance of the athletes during a game. In addition, industries could produce tools with high-tech aiding the athletes show performance over their abilities. For an account, in the swimming field, there could be fabricated swimming suites for minimizing the surface roughness and friction and increasing the performance of the swimmer beyond bare skin swimming. Therefore, the concept of the healthiness and fair competitions in the sports could be nullified with the high technology. The international sports laws limits the performance of the tools in sports to maintain the philosophy behind the sport games. On the other hand, these limitation should not affect the durability of the tools (Karami *et al*. 2019, Bellal *et al*. 2020, Menasria *et al*. 2020, Bakoura *et al*. 2021, Hachemi *et al*. 2021, Tahir *et al*. 2021, Zerrouki *et al*. 2021a, b).

Balls are important tools in many games ranging of various size, weight, material and applications. Balls could be found in table tennis games to golf and to basketball plays. In all these applications, standards apply to the characteristics of the balls. On the other hand, novel materials meeting the requirement and limitation of the standards could be utilized in the ball materials. New nanocomposite materials found applications in vast areas of today's life. One main application of the nanocomposite materials is in the field of sport. Arshid *et al*. (2021) examined three-layer sandwich nanocomposite structure for its vibrational responses in an elastic medium. In solving dynamics equations of complex composite structures and materials numerical methods are widely used (Bendenia *et al*. 2020, Heidari *et al*. 2021, Huang *et al*. 2021, Kumar *et al*. 2021, Van Vinh and Tounsi 2021, Zerrouki *et al*. 2021b). Several approaches with different advantages and disadvantages could be utilized in numerical solution of vibration problems. One of the most utilized methods is finite element method which is very effective in dealing with complicated geometries (Allam *et al*. 2020, Bekkaye *et al*. 2020, Bendenia *et al*. 2020, Bakoura *et al*. 2021). However, this method requires high computational resources to solve a problem in an accurate way (Zerrouki *et al*. 2021a, b, Wang *et al*. 2023b, Wang and Sigmund 2023). One another method is finite difference method for complicated geometries. However, with emerge of finite element method, the outdated finite difference solution is barely used nowadays. For structures with fairly simple geometries, the differential quadrature method is utilized widely in solving eigenvalue and nonlinear problems (Habibi *et al*. 2019a, 2021b, Al-Furjan *et al*. 2020b, 2021a). Beside high efficacy in solving nonlinear equations in a

*Corresponding author, Ph.D.,
E-mail: songzhiqiang@sdpei.edu.cn

ISSN: 2287-237X (Print), 2287-2388 (Online)

lower time and computational costs than other numerical methods, the DQM could provide satisfactory accurate results in buckling, vibration and nonlinear dynamic problems (Al-Furjan *et al*. 2021b, Safarpour *et al*. 2021, Xu *et al*. 2021).

Buckling analysis in nanocomposite structural components are also important in sport balls since in several occasion buckling would occur in these structures (Ebrahimi and Barati 2016, Matouk *et al*. 2020, Hadji and Avcar 2021, Kumar *et al*. 2021, Soleimani-Javid *et al*. 2021, Zhao *et al*. 2024). Zhang and Yu (2012) considered the buckling occurrence in table tennis balls under dynamic loading conditions. They also simulated the buckling forces and shapes using finite element numerical methods. The results of their study indicated that visco-elastic effects in impact loading conditions play important role in the energy absorption of the tennis balls. Hutchinson (Hutchinson 2016) reviewed the buckling studies on the spherical structures made of conventional materials. In the review, the main focus was on the analytical solutions of the buckling for both perfect and imperfect spherical shell structures. Habibi *et al*. (2019c) examined the buckling modes in imperfect shell structures made of nanocomposite materials. In their analyses, differential quadrature method was utilized to obtain the numerical solution of the governing equations of a functionally graded structure. The study was limited to the cylindrical shell structures. In another study Ebrahimi *et al*. (2019b) considered dynamic buckling in a cylindrical shell under the influence of the gyroscopic loads from spinning of the structure. They found, through numerical analysis, that the buckling critical load is highly dependent on the material properties as well as spinning velocity of the structure. Li *et al*. (2020) also examined buckling condition in nanocomposite shell structures using scale dependent elasticity theories. They included thermal loading effects in obtaining dynamic deflection and instability in the cylindrical shell structure.

In nano-scale structure and in parts composed of nano-size particles, conventional continuum mechanics theories are no capable of reflecting the most important features of the mechanical responses of the structure, i.e., size dependency. Size dependent properties of metals are a well-known properties for metallurgists since the yield strength is strongly dependent on the grain size of the metals in the annealed conditions. Other studies also confirms the dependency of the mechanical properties on the size of grains in small scales (Amelirad and Assempour 2019, 2021). Similar dependency on the microstructure length scale is observed in nanomaterials for different micro/nano effects. Therefore, with the assumption of continuity of small scale structures, it is more convenient to exploit scale dependent elasticity theories to have an insight into effects of small scale features like size of reinforcement particles and microcracks in composite materials. In this regard, several size-dependent theories to be utilized in small-scales have been proposed. The well-known nonlocal elasticity theory has been utilized in vibrational analysis of nanocomposite structures (Moayedi *et al*. 2019, Al-Furjan *et al*. 2020a). Other theories that are frequently used in small-scale analyses is strain gradient theory (Habibi *et al*. 2021a, Zhang *et al*. 2021, Al-Furjan *et al*. 2022), couple stress theory (Ghabussi *et al*. 2021, Liu *et al*. 2021b, Shamsaddini Lori *et al*. 2021, Shariati *et al*. 2021) and combinations of these theories (Ebrahimi *et al*. 2020, Ghabussi *et al*. 2020, Lori *et al*. 2020, Shi *et al*. 2020).

The observations of the natural frequency in engineering materials and spherical structures could not be easily generalized to balls in sport. One important feature of ball mechanics in a game in the large deformation they endure in contrast to the small deformations in the other structures. On the other hand, effect of internal pressure is disregarded in most calculations where it has an influential role in determining vibration and other mechanical properties of the balls. One another differences between ball and other engineering structures are the loading condition and state of t boundary conditions. The loading in the balls are mostly in the form impact loading and there are no detectable boundary conditions in a free ball. Therefore, in the analyses, some tricks have to be adopted to apply boundary conditions in mechanical analyses of the balls in sports. Zhang and Yu (2012) experimentally examined the condition of buckling in ping-pong balls using both quasi-static and impact loading conditions. The state of buckling as well as the mode shape of buckling during several tests were measured and simulated. The numerical simulations were similar to the experimental results in the condition of incorporating viscoelasticity properties of the ball. The dynamic buckling condition of sport balls with different materials and thicknesses were examined by Cross (Cross 2014). In another experimental examination of buckling condition in the ping-pong balls, Rémond *et al*. (2022) found that initiation of buckling occurs when deflection of the shell exceeds twice the thickness of the ball in both quasi-static and dynamic loadings. Moreover, they found that the most energy dissipation in the ball impact is due to friction energy loss. Asai *et al*. (2007) considered instability of ball in the air due to aerodynamic forces. They observed some phenomena in the air flow around soccer ball which were different from other balls with smooth and non-smooth surface conditions.

The unique demands placed on sports balls necessitate a departure from conventional engineering analyses. Unlike static structures or machine components, sports balls are subjected to dynamic, high-impact forces, often involving significant deformations. This dynamic loading regime introduces complexities that are not readily addressed by traditional linear elastic models. Furthermore, the interplay between material properties and aerodynamic forces becomes paramount. The spin imparted on a ball, for instance, significantly alters its trajectory due to the Magnus effect, a phenomenon that is highly sensitive to the ball's surface texture and aerodynamic properties. Additionally, the viscoelastic nature of the materials used in sports balls, which is often temperature-dependent, further complicates the analysis. These factors must be considered to accurately predict the performance of a sports ball under varying environmental and playing conditions. The design of a sport ball requires a multi-physics approach, considering structural mechanics, fluid dynamics, and material science, in order to create a model that accurately predicts the real world behavior of a ball.

Moreover, the human factor adds a layer of complexity not typically encountered in traditional engineering design. The tactile feedback perceived by the player is influenced by the ball's surface texture, stiffness, and damping characteristics, which in turn affects their performance. Consequently, the development of sports balls requires a multidisciplinary approach that integrates material science, biomechanics, and fluid dynamics, as well as considering the player's sensory experience. The interaction between the ball and the playing surface or the player's hand introduces further complexities that are often overlooked in conventional engineering analyses. The coefficient of restitution, which dictates the energy loss during impact, is highly dependent on the surface properties of both the ball and the contact surface. Surface roughness, material compliance, and impact velocity all play crucial roles in determining the rebound characteristics. This holistic approach ensures that the design of sports balls not only optimizes performance but also enhances the player's comfort and control. This research aims to contribute to this understanding by analyzing the vibrational characteristics of nanocomposite volleyballs, considering the unique loading conditions and material properties inherent in sports ball design.

This study investigates the vibrational response of a graphene oxide-reinforced volleyball under impact loading, aiming to enhance its dynamic stability. Employing Hamilton's principle and spherical shell coordinates, we derive the governing equations for the ball's motion under internal loading. These equations are solved using the generalized differential quadrature (GDQ) method and analytical techniques to analyze the vibrational modes. The results demonstrate a significant correlation between the ball's radius and its dynamic stability, with variations in radius substantially affecting vibrational characteristics. Notably, we find that increased ball mass, independent of size, contributes to enhanced stability upon ground impact. This observation suggests that heavier balls exhibit improved resistance to deformation and vibration, leading to more predictable trajectories. The findings provide a quantitative basis for optimizing volleyball design by elucidating the interplay between material reinforcement, geometry, and impact dynamics, thereby facilitating the development of volleyballs with improved stability and performance.

2. Underlying equations

This study utilizes a functionally graded graphene oxide powder-reinforced composite (FG-GOPRC) spherical shell as the primary model for analysis. To accurately represent the material distribution, Fig. 1 illustrates the geometric configuration of the spherical shell, alongside various distribution patterns of the graphene oxide powders (GOPs) across the shell's thickness.

It is essential to clarify the geometric parameters depicted in Fig. 1. The green arrows in the illustration denote the outer and inner radii of the spherical shell, respectively. These dimensions are critical for accurately defining the shell's geometry and subsequent analysis. To

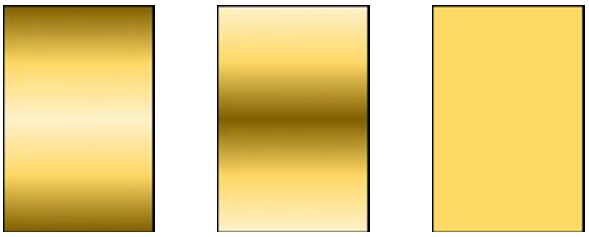

(a) GOP-X (b) GOP-O (c) GOP-UD

Fig. 1 Illustration depicting various graphene platelet (GPL) distribution patterns within the composite material

determine the effective material properties of the FG-GOPRC spherical shell, we employed the Halpin-Tsai homogenization method. This method is particularly suitable for predicting the mechanical properties of composite materials, such as Young's modulus, by considering the properties of the individual constituents (i.e., the base material and the graphene oxide powders) and their volume fractions. Specifically, the Halpin-Tsai method allows us to calculate the effective Young's modulus of the composite material as a function of the GOP distribution patterns illustrated in Fig. 1, thereby providing a robust foundation for our dynamic analysis (Zhang *et al*. 2020):

$$\begin{aligned}\mathcal{E} = 0.49 \times \frac{1+\mathbb{q}_L \mathfrak{Y}_L \mathcal{V}_{GOP}}{1-\mathfrak{Y}_L \mathcal{V}_{GOP}} \times \mathcal{E}_m \\ +0.51 \times \frac{1+\mathbb{q}_{\mathbb{q}\mathfrak{Y}} \mathfrak{Y}_{\mathfrak{Y}} \mathcal{V}_{GOP}}{1-\mathfrak{Y}_{\mathfrak{Y}} \mathcal{V}_{GOP}} \times \mathcal{E}_m\end{aligned} \tag{1}$$

in which, $\mathbb{q}_L = \mathbb{q}_{\mathfrak{Y}} = 2\frac{d_{GOP}}{h_{GOP}}$, $\mathcal{V}^*_{GOP} = \frac{W_{GOP}}{\mathbb{W}_{GOP}+\left(\frac{\rho_{GPL}}{\rho_m}\right)(1-\mathbb{W}_{GOP})}$, $\mathfrak{Y}_l = -\frac{1-\left(\frac{\mathcal{E}_{GOP}}{\mathcal{E}_m}\right)}{\mathbb{q}_l+\left(\frac{\mathcal{E}_{GOP}}{\mathcal{E}_m}\right)}$ and $\mathfrak{Y}_{\mathfrak{Y}} = -\frac{1-\left(\frac{\mathcal{E}_{GOP}}{\mathcal{E}_m}\right)}{\mathbb{q}_{\mathfrak{Y}}+\left(\frac{\mathcal{E}_{GOP}}{\mathcal{E}_m}\right)}$.

In addition to Young's modulus (Ge *et al*. 2023, Habibi *et al*. 2024, He *et al*. 2024, Huang *et al*. 2024, Jin *et al*. 2024, Li *et al*. 2024, Man *et al*. 2024, Wang *et al*. 2024a, b, Zhang *et al*. 2024b, c, Zhao *et al*. 2024), the effective density and Poisson's ratio of the FG-GOPRC material were crucial for the dynamic analysis. These properties were calculated using the same Halpin-Tsai homogenization method. The resulting values are presented below: Also, the density as well as Poisson's ratio are as follows:

$$\begin{aligned}\rho = \rho_{GOP}\mathcal{V}_{GOP} + \rho_m(1-\mathcal{V}_{GOP}), \\ \nu = \nu_{GOP}\mathcal{V}_{GOP} + \nu_m(1-\mathcal{V}_{GOP})\end{aligned} \tag{2}$$

The shear modulus of the FG-GOPRC system was subsequently derived using the established relationships between elastic moduli, as follows:

$$G = \frac{\mathcal{E}}{2(1+\nu)} \tag{3}$$

Finally, the various distribution patterns of graphene oxide powders (GOPs) within the spherical shell's thickness were defined as follows (Zhang *et al*. 2020):

$$\mathcal{V}_{GOP}(k) = 2\mathcal{V}^*_{GOP}\left(\frac{|2k-N_L-1|}{N_L}\right) \quad GOP\text{-}X, \tag{4a}$$

$$\mathcal{V}_{GOP}(k) = 2\mathcal{V}^*_{GOP}\left(1-\frac{|N_L-2k+1|}{N_L}\right) \quad GOP\text{-}O, \tag{4b}$$

$$\mathcal{V}_{GOP}(k) = \mathcal{V}^{*}_{GOP} \quad GOP\text{-}UD. \tag{4c}$$

Here, $k = 1,2,3,\dots,N_L$.

2.1 Equation of motion

The displacement field of the spherical shell was defined using the following expressions:

$$\begin{aligned}\Re(\emptyset,\Theta,\mathbb{q},\mathcal{Y}) &= \Re_0(\emptyset,\Theta,\mathcal{Y}) + \mathbb{q}\Re_1(\emptyset,\Theta,\mathcal{Y}\mathcal{Y})\\ &+\mathbb{q}^2\Re_2(\emptyset,\Theta,\mathcal{Y}) + \mathbb{q}^3\Re_3(\emptyset,\Theta,\mathcal{Y})\\ &+\mathbb{q}^4\Re_4(\emptyset,\Theta,\mathcal{Y}) + \mathbb{q}^5\Re_5(\emptyset,\Theta,\mathcal{Y})\end{aligned} \tag{5a}$$

$$\begin{aligned}\mathfrak{S}(\emptyset,\Theta,\mathbb{q},\mathcal{Y}) &= \mathfrak{S}_0(\emptyset,\Theta,\mathcal{Y}) + \mathbb{q}\mathfrak{S}_1(\emptyset,\Theta,\mathcal{Y})\\ &+\mathbb{q}^2\mathfrak{S}_2(\emptyset,\Theta,\mathcal{Y}) + \mathbb{q}^3\mathfrak{S}_3(\emptyset,\Theta,\mathcal{Y})\\ &+\mathbb{q}^4\mathfrak{S}_4(\emptyset,\Theta,\mathcal{Y}) + \mathbb{q}^5\mathfrak{S}_5(\emptyset,\Theta,\mathcal{Y})\end{aligned} \tag{5b}$$

$$\begin{aligned}\mathfrak{T}(\emptyset,\Theta,\mathbb{q},\mathcal{Y}) &= \mathfrak{T}_0(\emptyset,\Theta,\mathcal{Y}) + \mathbb{q}\mathfrak{T}_1(\emptyset,\Theta,\mathcal{Y}) +\\ &\mathbb{q}^2\mathfrak{T}_2(\emptyset,\Theta,\mathcal{Y}) + \mathbb{q}^3\mathfrak{T}_3(\emptyset,\Theta,\mathcal{Y})\\ &+\mathbb{q}^4\mathfrak{T}_4(\emptyset,\Theta,\mathcal{Y}) + \mathbb{q}^5\mathfrak{T}_5(\emptyset,\Theta,\mathcal{Y})\end{aligned} \tag{5c}$$

The strain components (Wang *et al*. 2023a, Alam *et al*. 2025, Yang *et al*. 2025), expressed as functions of the displacement field, were defined by the following strain-displacement relationships:

$$\begin{aligned}&\mathfrak{g}_{\emptyset\emptyset} = \frac{\partial\Re}{\mathrm{r}\,\partial\emptyset} + \frac{\mathfrak{T}}{\mathrm{r}}, \quad \mathfrak{g}_{\Theta\Theta} = \frac{\partial\mathfrak{S}}{\mathrm{r}_1\,\partial\Theta} + \frac{\Re}{\mathrm{r}\mathrm{r}_1}\frac{\partial R_1}{\partial\emptyset} + \frac{\mathfrak{T}}{\mathrm{r}},\\ &\mathfrak{g}_{\mathbb{q}\mathbb{q}} = \frac{\partial\mathfrak{T}}{\partial\mathbb{q}}\\ &\mathfrak{g}_{\emptyset\Theta} = \frac{\partial\mathfrak{S}}{\mathrm{r}\,\partial\emptyset} - \frac{\mathfrak{S}}{\mathrm{r}\mathrm{r}_1}\frac{\partial R_1}{\partial\emptyset} + \frac{\partial\Re}{\mathrm{r}_1\,\partial\Theta},\\ &\mathfrak{g}\ \mathfrak{g}_{\emptyset\mathbb{q}} = \frac{\partial\Re}{\partial\mathbb{q}} - \frac{\Re}{\mathrm{r}} + \frac{\partial\mathfrak{T}}{\mathrm{r}\,\partial\emptyset},\ \mathfrak{g}_{\Theta\mathbb{q}} = \frac{\partial\mathfrak{S}}{\partial\mathbb{q}} - \frac{\mathfrak{S}}{\mathrm{r}} + \frac{\partial\mathfrak{T}}{\mathrm{r}_1\,\partial\Theta}\end{aligned} \tag{6}$$

By substituting $\mathrm{r}_1 = \mathrm{r}\sin\emptyset$ in Eq. (6)

$$\begin{aligned}&\mathfrak{g}_{\emptyset\emptyset} = \frac{\partial\Re}{\mathrm{r}\,\partial\emptyset} + \frac{\mathfrak{T}}{\mathrm{r}},\\ &\mathfrak{g}_{\Theta\Theta} = \frac{1}{\mathrm{r}\sin(\emptyset)}\frac{\partial\mathfrak{S}}{\partial\Theta} + \frac{\cot(\emptyset)\Re}{\mathrm{r}} + \frac{\mathfrak{T}}{\mathrm{r}}, \quad \mathfrak{g}_{\mathbb{q}\mathbb{q}} = \frac{\partial\mathfrak{T}}{\partial\mathbb{q}}\end{aligned}$$

$$\begin{aligned}&\mathfrak{g}_{\emptyset\Theta} = \frac{\partial\mathfrak{S}}{\mathrm{r}\,\partial\emptyset} - \frac{\cot(\emptyset)\mathfrak{S}}{\mathrm{r}} + \frac{1}{\mathrm{r}\sin(\emptyset)}\frac{\partial\Re}{\partial\Theta},\\ &\mathfrak{g}_{\emptyset\mathbb{q}} = \frac{\partial\Re}{\partial\mathbb{q}} - \frac{\Re}{\mathrm{r}} + \frac{\partial\mathfrak{T}}{\mathrm{r}\,\partial\emptyset},\\ &\mathfrak{g}_{\Theta z} = \frac{\partial\mathfrak{S}}{\partial\mathbb{q}} - \frac{\mathfrak{S}}{\mathrm{r}} + \frac{1}{\mathrm{r}\sin(\emptyset)}\frac{\partial\mathfrak{T}}{\partial\Theta}\end{aligned} \tag{7}$$

where

$$\mathfrak{g}_{\emptyset\emptyset} = \mathfrak{g}^{(0)}_{\emptyset\emptyset} + \mathbb{q}\mathfrak{g}^{(1)}_{\emptyset\emptyset} + \mathbb{q}^2\mathfrak{g}^{(2)}_{\emptyset\emptyset} + \mathbb{q}^3\mathfrak{g}^{(3)}_{\emptyset\emptyset} + \mathbb{q}^4\mathfrak{g}^{(4)}_{\emptyset\emptyset} + \mathbb{q}^5\mathfrak{g}^{(5)}_{\emptyset\emptyset}$$

$$\mathfrak{g}_{\Theta\Theta} = \mathfrak{g}^{(0)}_{\Theta\Theta} + \mathbb{q}\mathfrak{g}^{(1)}_{\Theta\Theta} + \mathbb{q}^2\mathfrak{g}^{(2)}_{\Theta\Theta} + \mathbb{q}^3\mathfrak{g}^{(3)}_{\Theta\Theta} + \mathbb{q}^4\mathfrak{g}^{(4)}_{\Theta\Theta} + \mathbb{q}^5\mathfrak{g}^{(5)}_{\Theta\Theta} \tag{8}$$

$$\mathfrak{g}_{\mathbb{q}\mathbb{q}} = \mathfrak{g}^{(0)}_{\mathbb{q}\mathbb{q}} + \mathbb{q}\mathfrak{g}^{(1)}_{\mathbb{q}\mathbb{q}} + \mathbb{q}^2\mathfrak{g}^{(2)}_{\mathbb{q}\mathbb{q}} + \mathbb{q}^3\mathfrak{g}^{(3)}_{\mathbb{q}\mathbb{q}} + \mathbb{q}^4\mathfrak{g}^{(4)}_{\mathbb{q}\mathbb{q}} + \mathbb{q}^5\mathfrak{g}^{(5)}_{\mathbb{q}\mathbb{q}}$$

$$\mathfrak{g}_{\emptyset\mathbb{q}} = \mathfrak{g}^{(0)}_{\emptyset\mathbb{q}} + \mathbb{q}\mathfrak{g}^{(1)}_{\emptyset\mathbb{q}} + \mathbb{q}^2\mathfrak{g}^{(2)}_{\emptyset\mathbb{q}} + \mathbb{q}^3\mathfrak{g}^{(3)}_{\emptyset\mathbb{q}} + \mathbb{q}^4\mathfrak{g}^{(4)}_{\emptyset\mathbb{q}} + \mathbb{q}^5\mathfrak{g}^{(5)}_{\emptyset\mathbb{q}}$$

$$\mathfrak{g}_{\Theta\mathbb{q}} = \mathfrak{g}^{(0)}_{\Theta\mathbb{q}} + \mathbb{q}\mathfrak{g}^{(1)}_{\Theta\mathbb{q}} + \mathbb{q}^2\mathfrak{g}^{(2)}_{\Theta\mathbb{q}} + \mathbb{q}^3\mathfrak{g}^{(3)}_{\Theta\mathbb{q}} + \mathbb{q}^4\mathfrak{g}^{(4)}_{\Theta\mathbb{q}} + \mathbb{q}^5\mathfrak{g}^{(5)}_{\Theta\mathbb{q}}$$

$$\mathfrak{g}_{\emptyset\Theta} = \mathfrak{g}^{(0)}_{\emptyset\Theta} + \mathbb{q}\mathfrak{g}^{(1)}_{\emptyset\Theta} + \mathbb{q}^2\mathfrak{g}^{(2)}_{\emptyset\Theta} + \mathbb{q}^3\mathfrak{g}^{(3)}_{\emptyset\Theta} + \mathbb{q}^4\mathfrak{g}^{(4)}_{\emptyset\Theta} + \mathbb{q}^5\mathfrak{g}^{(5)}_{\emptyset\Theta}$$

where

$$\begin{aligned}&\mathfrak{g}^{(0)}_{\emptyset\emptyset} = \frac{\partial\Re_0}{\mathrm{r}\,\partial\emptyset} + \frac{\mathfrak{T}_0}{\mathrm{r}}, \mathfrak{g}^{(1)}_{\emptyset\emptyset} = \frac{\partial\Re_1}{\mathrm{r}\,\partial\emptyset} + \frac{\mathfrak{T}_1}{\mathrm{r}},\\ &\mathfrak{g}^{(2)}_{\emptyset\emptyset} = \frac{\partial\Re_2}{\mathrm{r}\,\partial\emptyset} + \frac{\mathfrak{T}_2}{\mathrm{r}}, \mathfrak{g}^{(3)}_{\emptyset\emptyset} = \frac{\partial\Re_3}{\mathrm{r}\,\partial\emptyset} + \frac{\mathfrak{T}_3}{\mathrm{r}}\end{aligned}$$

$$\mathfrak{g}^{(4)}_{\emptyset\emptyset} = \frac{\partial\Re_4}{\mathrm{r}\,\partial\emptyset} + \frac{\mathfrak{T}_4}{\mathrm{r}}, \qquad \mathfrak{g}^{(5)}_{\emptyset\emptyset} = \frac{\partial\Re_5}{\mathrm{r}\,\partial\emptyset} + \frac{\mathfrak{T}_5}{\mathrm{r}}$$

$$\begin{aligned}&\mathfrak{g}^{(0)}_{\Theta\Theta} = \frac{1}{\mathrm{r}\sin(\emptyset)}\frac{\partial\mathfrak{S}_0}{\partial\Theta} + \frac{\cot(\emptyset)\Re_0}{\mathrm{r}} + \frac{\mathfrak{T}_0}{\mathrm{r}},\\ &\mathfrak{g}^{(1)}_{\Theta\Theta} = \frac{1}{\mathrm{r}\sin(\emptyset)}\frac{\partial\mathfrak{S}_1}{\partial\Theta} + \frac{\cot(\emptyset)\Re_1}{\mathrm{r}} + \frac{\mathfrak{T}_2}{\mathrm{r}}\end{aligned}$$

$$\begin{aligned}&\mathfrak{g}^{(2)}_{\Theta\Theta} = \frac{1}{\mathrm{r}\sin(\emptyset)}\frac{\partial\mathfrak{S}_2}{\partial\Theta} + \frac{\cot(\emptyset)\Re_2}{\mathrm{r}} + \frac{\mathfrak{T}_2}{\mathrm{r}},\\ &\mathfrak{g}^{(3)}_{\Theta\Theta} = \frac{1}{\mathrm{r}\sin(\emptyset)}\frac{\partial\mathfrak{S}_3}{\partial\Theta} + \frac{\cot(\emptyset)\Re_3}{\mathrm{r}} + \frac{\mathfrak{T}_3}{\mathrm{r}}\end{aligned}$$

$$\begin{aligned}&\mathfrak{g}^{(4)}_{\Theta\Theta} = \frac{1}{\mathrm{r}\sin(\emptyset)}\frac{\partial\mathfrak{S}_4}{\partial\Theta} + \frac{\cot(\emptyset)\Re_4}{\mathrm{r}} + \frac{\mathfrak{T}_4}{\mathrm{r}},\\ &\mathfrak{g}^{(5)}_{\Theta\Theta} = \frac{1}{\mathrm{r}\sin(\emptyset)}\frac{\partial\mathfrak{S}_5}{\partial\Theta} + \frac{\cot(\emptyset)\Re_5}{\mathrm{r}} + \frac{\mathfrak{T}_5}{\mathrm{r}}\end{aligned}$$

$$\begin{aligned}&\mathfrak{g}^{(0)}_{\mathbb{q}\mathbb{q}} = \mathfrak{T}_1,\ \mathfrak{g}^{(1)}_{\mathbb{q}\mathbb{q}} = 2\mathfrak{T}_2,\ \mathfrak{g}^{(2)}_{\mathbb{q}\mathbb{q}} = 3\mathfrak{T}_3,\\ &\mathfrak{g}^{(3)}_{\mathbb{q}\mathbb{q}} = 4\mathfrak{T}_4, \qquad \mathfrak{g}^{(4)}_{\mathbb{q}\mathbb{q}} = 5\mathfrak{T}_5, \qquad \mathfrak{g}^{(5)}_{\mathbb{q}\mathbb{q}} = 0\end{aligned} \tag{9}$$

$$\begin{aligned}&\mathfrak{g}^{(0)}_{\emptyset\mathbb{q}} = \frac{\partial\mathfrak{S}_0}{\mathrm{r}\,\partial\emptyset} - \frac{\cot(\emptyset)\mathfrak{S}_0}{\mathrm{r}} + \frac{1}{\mathrm{r}\sin(\emptyset)}\frac{\partial\Re_0}{\partial\Theta},\\ &\mathfrak{g}^{(1)}_{\emptyset\mathbb{q}} = \frac{\partial\mathfrak{S}_1}{\mathrm{r}\,\partial\emptyset} - \frac{\cot(\emptyset)\mathfrak{S}_1}{\mathrm{r}} + \frac{1}{\mathrm{r}\sin(\emptyset)}\frac{\partial\Re_1}{\partial\Theta}\end{aligned}$$

$$\begin{aligned}&\mathfrak{g}^{(2)}_{\emptyset\mathbb{q}} = \frac{\partial\mathfrak{S}_2}{\mathrm{r}\,\partial\emptyset} - \frac{\cot(\emptyset)\mathfrak{S}_2}{\mathrm{r}} + \frac{1}{\mathrm{r}\sin(\emptyset)}\frac{\partial\Re_2}{\partial\Theta},\\ &\mathfrak{g}^{(3)}_{\emptyset\mathbb{q}} = \frac{\partial\mathfrak{S}_3}{\mathrm{r}\,\partial\emptyset} - \frac{\cot(\emptyset)\mathfrak{S}_3}{\mathrm{r}} + \frac{1}{\mathrm{r}\sin(\emptyset)}\frac{\partial\Re_3}{\partial\Theta}\end{aligned}$$

$$\begin{aligned}&\mathfrak{g}^{(4)}_{\emptyset\mathbb{q}} = \frac{\partial\mathfrak{S}_4}{\mathrm{r}\,\partial\emptyset} - \frac{\cot(\emptyset)\mathfrak{S}_4}{\mathrm{r}} + \frac{1}{\mathrm{r}\sin(\emptyset)}\frac{\partial\Re_4}{\partial\Theta},\\ &\mathfrak{g}^{(5)}_{\emptyset\mathbb{q}} = \frac{\partial\mathfrak{S}_5}{\mathrm{r}\,\partial\emptyset} - \frac{\cot(\emptyset)\mathfrak{S}_5}{\mathrm{r}} + \frac{1}{\mathrm{r}\sin(\emptyset)}\frac{\partial\Re_5}{\partial\Theta}\end{aligned}$$

$$\begin{aligned}&\mathfrak{g}^{(0)}_{\emptyset\mathbb{q}} = \Re_1 - \frac{\Re_0}{\mathrm{r}} + \frac{\partial\mathfrak{T}_0}{\mathrm{r}\,\partial\emptyset},\\ &\mathfrak{g}^{(1)}_{\emptyset\mathbb{q}} = 2\Re_2 - \frac{\Re_1}{\mathrm{r}} + \frac{\partial\mathfrak{T}_1}{\mathrm{r}\,\partial\emptyset},\end{aligned}$$

$$\mathfrak{g}_{\emptyset\mathfrak{q}}^{(2)} = 3\Re_3 - \frac{\Re_2}{\mathrm{r}} + \frac{\partial \mathfrak{T}_2}{\mathrm{r}\,\partial \emptyset},$$
$$\mathfrak{g}_{\emptyset z}^{(3)} = 4\Re_4 - \frac{\Re_3}{\mathrm{r}} + \frac{\partial \mathfrak{T}_3}{\mathrm{r}\,\partial \emptyset},$$
$$\mathfrak{g}_{\emptyset z}^{(4)} = 5\Re_5 - \frac{\Re_4}{\mathrm{r}} + \frac{\partial \mathfrak{T}_4}{\mathrm{r}\,\partial \emptyset}$$
$$\mathfrak{g}_{\emptyset z}^{(5)} = -\frac{\Re_5}{\mathrm{r}} + \frac{\partial \mathfrak{T}_5}{\mathrm{r}\,\partial \emptyset}$$

$$\mathfrak{g}_{\emptyset\Theta}^{(0)} = \Im_1 - \frac{\Im_0}{\mathrm{r}} + \frac{1}{\mathrm{r}\sin(\emptyset)}\frac{\partial \mathfrak{T}_0}{\partial \Theta},$$
$$\mathfrak{g}_{\emptyset\Theta}^{(1)} = 2\Im_2 - \frac{\Im_1}{\mathrm{r}} + \frac{1}{\mathrm{r}\sin(\emptyset)}\frac{\partial \mathfrak{T}_1}{\partial \Theta}$$

$$\mathfrak{g}_{\emptyset\Theta}^{(2)} = 3\Im_3 - \frac{\Im_2}{\mathrm{r}} + \frac{1}{\mathrm{r}\sin(\emptyset)}\frac{\partial \mathfrak{T}_2}{\partial \Theta},$$
$$\mathfrak{g}_{\emptyset\Theta}^{(3)} = 4\Im_4 - \frac{\Im_3}{\mathrm{r}} + \frac{1}{\mathrm{r}\sin(\emptyset)}\frac{\partial \mathfrak{T}_3}{\partial \Theta}$$

$$\mathfrak{g}_{\emptyset\Theta}^{(4)} = 5\Im_5 - \frac{\Im_4}{\mathrm{r}} + \frac{1}{\mathrm{r}\sin(\emptyset)}\frac{\partial \mathfrak{T}_4}{\partial \Theta},$$
$$\mathfrak{g}_{\emptyset\Theta}^{(5)} = \frac{\Im_5}{\mathrm{r}} + \frac{1}{\mathrm{r}\sin(\emptyset)}\frac{\partial \mathfrak{T}_5}{\partial \Theta}$$

For the elastic system we have:

$$\begin{aligned}
\aleph_{\emptyset\emptyset} &= \left(\mathring{\mathrm{A}}_{11}\mathfrak{g}_{\emptyset\emptyset} + \mathring{\mathrm{A}}_{12}\mathfrak{g}_{\Theta\Theta} + \mathring{\mathrm{A}}_{13}\mathfrak{g}_{\mathfrak{q}\mathfrak{q}}\right),\\
\aleph_{\Theta\Theta} &= \left(\mathring{\mathrm{A}}_{12}\mathfrak{g}_{\emptyset\emptyset} + \mathring{\mathrm{A}}_{22}\mathfrak{g}_{\Theta\Theta} + \mathring{\mathrm{A}}_{23}\mathfrak{g}_{\mathfrak{q}\mathfrak{q}}\right),\\
\aleph_{\mathfrak{q}\mathfrak{q}} &= \left(\mathring{\mathrm{A}}_{13}\mathfrak{g}_{\emptyset\emptyset} + \mathring{\mathrm{A}}_{23}\mathfrak{g}_{\Theta\Theta} + \mathring{\mathrm{A}}_{33}\mathfrak{g}_{\mathfrak{q}\mathfrak{q}}\right),\\
\aleph_{\Theta\mathfrak{q}} &= \left(\mathring{\mathrm{A}}_{44}\mathfrak{g}_{\Theta\mathfrak{q}}\right),\\
\aleph_{\emptyset\mathfrak{q}} &= \left(\mathring{\mathrm{A}}_{55}\mathfrak{g}_{\emptyset\mathfrak{q}}\right),\\
\aleph_{\emptyset\Theta} &= \left(\mathring{\mathrm{A}}_{66}\mathfrak{g}_{\emptyset\Theta}\right),
\end{aligned} \tag{10}$$

where

$$\mathring{\mathrm{A}}_{11} = \frac{\mathcal{E}(1-\nu)}{(1+\nu)(1-2\nu)},\ \mathring{\mathrm{A}}_{33} = \mathring{\mathrm{A}}_{22} = \mathring{\mathrm{A}}_{11},$$
$$\mathring{\mathrm{A}}_{12} = \frac{\mathcal{E}\nu}{(1+\nu)(1-2\nu)},\quad \mathring{\mathrm{A}}_{13} = \mathring{\mathrm{A}}_{23} = \mathring{\mathrm{A}}_{12}, \tag{11}$$
$$\mathring{\mathrm{A}}_{44} = \frac{\mathcal{E}}{2(1+\nu)},\quad \mathring{\mathrm{A}}_{66} = \mathring{\mathrm{A}}_{55} = \mathring{\mathrm{A}}_{44}.$$

The equations that describe the motion of a system are derived through the application of Hamilton's principle (Dai *et al*. 2023a, b, Gu *et al*. 2023, Li *et al*. 2023, Peng *et al*. 2023, Sabzevari *et al*. 2023, Shariati *et al*. 2023, Xiang *et al*. 2023, Yang *et al*. 2023, Zhang *et al*. 2023a, b, Zhao *et al*. 2023, Zheng *et al*. 2023). This principle provides a variational framework from which the dynamics of a system can be determined by finding the path that minimizes the action integral. By employing this approach, the governing equations of motion are obtained, offering a comprehensive description of the system's behavior.

$$\delta\int_{\mathfrak{Y}_1}^{\mathfrak{Y}_2}\left(\Pi_k - (\Pi_e + \Pi_w)\right)d\mathfrak{Y} = 0 \tag{12}$$

In these equations, Π_k denotes the kinetic energy, Π_e the potential energy, and Π_w the work performed by the system (Habibi *et al*. 2016, 2018a, b, 2019b, d, e, Ebrahimi *et al*. 2019a, Esmailpoor Hajilak *et al*. 2019, Pourjabari *et al*. 2019, Safarpour *et al*. 2019a, Zhu *et al*. 2022, Dai *et al*. 2023b, Lu *et al*. 2023a, b, Ma *et al*. 2023, Tang *et al*. 2023, Wang *et al*. 2023b, Zheng *et al*. 2023).The kinetic energy is indicated as follows:

$$\Pi_k = \int_V \frac{1}{2}\rho(\emptyset,\Theta,z)\left[\left(\frac{\partial \Re}{\partial \mathfrak{Y}}\right)^2 + \left(\frac{\partial \Im}{\partial \mathfrak{Y}}\right)^2 + \left(\frac{\partial \mathfrak{T}}{\partial \mathfrak{Y}}\right)^2\right]dV \tag{13}$$

The potential energy of the encompassing strain energy and potential from external forces, is expressed as follows:

$$\begin{aligned}
\Pi_u = \int_V \frac{1}{2}\big[&\aleph_{\emptyset\emptyset}\mathfrak{g}_{\emptyset\emptyset} + \aleph_{\Theta\Theta}\mathfrak{g}_{\Theta\Theta} + \aleph_{\mathfrak{q}\mathfrak{q}}\mathfrak{g}_{\mathfrak{q}\mathfrak{q}} + \aleph_{\Theta\mathfrak{q}}\mathfrak{g}_{\Theta\mathfrak{q}}\\
&+ \aleph_{\emptyset\mathfrak{q}}\mathfrak{g}_{\emptyset\mathfrak{q}} + \aleph_{\emptyset\Theta}\mathfrak{g}_{\emptyset\Theta}\big]\,dV
\end{aligned} \tag{14}$$

The work done by the system is expressed as follows:

$$\begin{aligned}
\Pi_u = \int_A \frac{\mathcal{P}}{2}\Bigg\{&\left\{\frac{1}{\mathrm{r}^2\sin(\emptyset)}\frac{\partial}{\partial \emptyset}\left(\sin(\emptyset)\frac{\partial \mathfrak{T}_0}{\partial \emptyset}\right)\right\}\\
&+ \frac{1}{\mathrm{r}^2\sin^2(\emptyset)}\frac{\partial^2 \mathfrak{T}_0}{\partial \Theta^2}\Bigg\}\,\mathfrak{T}_0 dA
\end{aligned} \tag{15}$$

where P indicates the In-plane mechanical loading.

By substituting the expressions for kinetic energy, potential energy, and work from Eqs. (13)-(15) into the governing principle in Eq. (12), we obtain the equations of motion.

The corresponding boundary conditions are defined as

$$\begin{aligned}
&\left(\frac{\mathbb{N}_{\emptyset\emptyset}}{\mathrm{r}}\right)\widehat{\sigma}_{\emptyset} + \left(\frac{\mathbb{N}_{\emptyset\Theta}}{\mathrm{r}\sin(\emptyset)}\right)\widehat{\sigma}_{\Theta} = 0,\\
&\left(\frac{\mathbb{N}_{\emptyset\Theta}}{\mathrm{r}}\right)\widehat{\sigma}_{\emptyset} + \left(\frac{\mathbb{N}_{\Theta\Theta}}{\mathrm{r}\sin(\emptyset)}\right)\widehat{\sigma}_{\Theta} = 0,\\
&\left(\frac{\mathbb{N}_{\emptyset z}}{\mathrm{r}}\right)\widehat{\sigma}_{\emptyset} + \left(\frac{\mathbb{N}_{\Theta\mathfrak{q}}}{\mathrm{r}\sin(\emptyset)}\right)\widehat{\sigma}_{\Theta} = 0,\\
&\left(\frac{\mathbb{M}_{\emptyset\emptyset}}{\mathrm{r}}\right)\widehat{\sigma}_{\emptyset} + \left(\frac{\mathbb{M}_{\emptyset\Theta}}{\mathrm{r}\sin(\emptyset)}\right)\widehat{\sigma}_{\Theta} = 0,\\
&\left(\frac{\mathbb{M}_{\emptyset\Theta}}{\mathrm{r}}\right)\widehat{\sigma}_{\emptyset} + \left(\frac{\mathbb{M}_{\Theta\Theta}}{\mathrm{r}\sin(\emptyset)}\right)\widehat{\sigma}_{\Theta} = 0,\\
&\left(\frac{\mathbb{M}_{\emptyset\mathfrak{q}}}{\mathrm{r}}\right)\widehat{\sigma}_{\emptyset} + \left(\frac{\mathbb{M}_{\Theta\mathfrak{q}}}{\mathrm{r}\sin(\emptyset)}\right)\widehat{\sigma}_{\Theta} = 0,\\
&\left(\frac{\mathbb{P}_{\emptyset\emptyset}}{\mathrm{r}}\right)\widehat{\sigma}_{\emptyset} + \left(\frac{\mathbb{P}_{\emptyset\Theta}}{\mathrm{r}\sin(\emptyset)}\right)\widehat{\sigma}_{\Theta} = 0,\\
&\left(\frac{\mathbb{P}_{\emptyset\Theta}}{\mathrm{r}}\right)\widehat{\sigma}_{\emptyset} + \left(\frac{\mathbb{P}_{\Theta\Theta}}{\mathrm{r}\sin(\emptyset)}\right)\widehat{\sigma}_{\Theta} = 0,\\
&\left(\frac{\mathbb{P}_{\emptyset z}}{\mathrm{r}}\right)\widehat{\sigma}_{\emptyset} + \left(\frac{\mathbb{P}_{\Theta\mathfrak{q}}}{\mathrm{r}\sin(\emptyset)}\right)\widehat{\sigma}_{\Theta} = 0,\\
&\left(\frac{\mathbb{Q}_{\emptyset\emptyset}}{\mathrm{r}}\right)\widehat{\sigma}_{\emptyset} + \left(\frac{\mathbb{Q}_{\emptyset\Theta}}{\mathrm{r}\sin(\emptyset)}\right)\widehat{\sigma}_{\Theta} = 0,
\end{aligned} \tag{16}$$

$$\left(\frac{\mathbb{Q}_{\emptyset\Theta}}{\mathrm{r}}\right)\widehat{\sigma}_{\emptyset}+\left(\frac{\mathbb{Q}_{\Theta\Theta}}{\mathrm{rsin}(\emptyset)}\right)\widehat{\sigma}_{\Theta}=0,$$

$$\left(\frac{\mathbb{Q}_{\emptyset\mathbb{q}}}{\mathrm{r}}\right)\widehat{\sigma}_{\emptyset}+\left(\frac{\mathbb{Q}_{\Theta\mathbb{q}}}{\mathrm{rsin}(\emptyset)}\right)\widehat{\sigma}_{\Theta}=0,$$

$$\left(\frac{\mathbb{R}_{\emptyset\emptyset}}{\mathrm{r}}\right)\widehat{\sigma}_{\emptyset}+\left(\frac{\mathbb{R}_{\emptyset\Theta}}{\mathrm{rsin}(\emptyset)}\right)\widehat{\sigma}_{\Theta}=0,$$

$$\left(\frac{\mathbb{R}_{\emptyset\Theta}}{\mathrm{r}}\right)\widehat{\sigma}_{\emptyset}+\left(\frac{\mathbb{R}_{\Theta\Theta}}{\mathrm{rsin}(\emptyset)}\right)\widehat{\sigma}_{\Theta}=0,$$

$$\left(\frac{\mathbb{R}_{\emptyset\mathbb{q}}}{\mathrm{r}}\right)\widehat{\sigma}_{\emptyset}+\left(\frac{\mathbb{R}_{\Theta\mathbb{q}}}{\mathrm{rsin}(\emptyset)}\right)\widehat{\sigma}_{\Theta}=0,$$

$$\left(\frac{\mathbb{S}_{\emptyset\emptyset}}{\mathrm{r}}\right)\widehat{\sigma}_{\emptyset}+\left(\frac{\mathbb{S}_{\emptyset\Theta}}{\mathrm{rsin}(\emptyset)}\right)\widehat{\sigma}_{\Theta}=0,$$

$$\left(\frac{\mathbb{S}_{\emptyset\Theta}}{\mathrm{r}}\right)\widehat{\sigma}_{\emptyset}+\left(\frac{\mathbb{S}_{\Theta\Theta}}{\mathrm{rsin}(\emptyset)}\right)\widehat{\sigma}_{\Theta}=0,$$

$$\left(\frac{\mathbb{S}_{\emptyset\mathbb{q}}}{\mathrm{r}}\right)\widehat{\sigma}_{\emptyset}+\left(\frac{\mathbb{S}_{\Theta\mathbb{q}}}{\mathrm{rsin}(\emptyset)}\right)\widehat{\sigma}_{\Theta}=0.$$

where

$$\begin{Bmatrix}\mathbb{N}_{\emptyset\emptyset}\\ \mathbb{N}_{\Theta\Theta}\\ \mathbb{N}_{\mathbb{q}\mathbb{q}}\end{Bmatrix}=\int_V\begin{Bmatrix}\aleph_{\emptyset\emptyset}\\ \aleph_{\Theta\Theta}\\ \aleph_{\mathbb{q}\mathbb{q}}\end{Bmatrix}dV,$$

$$\begin{Bmatrix}\mathbb{M}_{\emptyset\emptyset}\\ \mathbb{M}_{\Theta\Theta}\\ \mathbb{M}_{\mathbb{q}\mathbb{q}}\end{Bmatrix}=\int_V\begin{Bmatrix}\mathbb{q}\aleph_{\emptyset\emptyset}\\ \mathbb{q}\aleph_{\Theta\Theta}\\ \mathbb{q}\aleph_{\mathbb{q}\mathbb{q}}\end{Bmatrix}dV,$$

$$\begin{Bmatrix}\mathbb{P}_{\emptyset\emptyset}\\ \mathbb{P}_{\Theta\Theta}\\ \mathbb{P}_{\mathbb{q}\mathbb{q}}\end{Bmatrix}=\int_V\begin{Bmatrix}\mathbb{q}^2\aleph_{\emptyset\emptyset}\\ \mathbb{q}^2\aleph_{\Theta\Theta}\\ \mathbb{q}^2\aleph_{\mathbb{q}\mathbb{q}}\end{Bmatrix}dV$$

$$\begin{Bmatrix}\mathbb{Q}_{\emptyset\emptyset}\\ \mathbb{Q}_{\Theta\Theta}\\ \mathbb{Q}_{\mathbb{q}\mathbb{q}}\end{Bmatrix}=\int_V\begin{Bmatrix}\mathbb{q}^3\aleph_{\emptyset\emptyset}\\ \mathbb{q}^3\aleph_{\Theta\Theta}\\ \mathbb{q}^3\aleph_{\mathbb{q}\mathbb{q}}\end{Bmatrix}dV,$$

$$\begin{Bmatrix}\mathbb{R}_{\emptyset\emptyset}\\ \mathbb{R}_{\Theta\Theta}\\ \mathbb{R}_{\mathbb{q}\mathbb{q}}\end{Bmatrix}=\int_V\begin{Bmatrix}\mathbb{q}^4\aleph_{\emptyset\emptyset}\\ \mathbb{q}^4\aleph_{\Theta\Theta}\\ \mathbb{q}^4\aleph_{\mathbb{q}\mathbb{q}}\end{Bmatrix}dV,$$

$$\begin{Bmatrix}\mathbb{S}_{\emptyset\emptyset}\\ \mathbb{S}_{\Theta\Theta}\\ \mathbb{S}_{\mathbb{q}\mathbb{q}}\end{Bmatrix}=\int_V\begin{Bmatrix}\mathbb{q}^5\aleph_{\emptyset\emptyset}\\ \mathbb{q}^5\aleph_{\Theta\Theta}\\ \mathbb{q}^5\aleph_{\mathbb{q}\mathbb{q}}\end{Bmatrix}dV$$

$$\begin{Bmatrix}\mathbb{N}_{\Theta\mathbb{q}}\\ \mathbb{N}_{\emptyset\mathbb{q}}\\ \mathbb{N}_{\emptyset\Theta}\end{Bmatrix}=\int_V\begin{Bmatrix}\aleph_{\Theta\mathbb{q}}\\ \aleph_{\emptyset\mathbb{q}}\\ \aleph_{\emptyset\Theta}\end{Bmatrix}dV,$$

$$\begin{Bmatrix}\mathbb{M}_{\Theta\mathbb{q}}\\ \mathbb{M}_{\emptyset\mathbb{q}}\\ \mathbb{M}_{\emptyset\Theta}\end{Bmatrix}=\int_V\begin{Bmatrix}\mathbb{q}\aleph_{\Theta\mathbb{q}}\\ \mathbb{q}\aleph_{\emptyset\mathbb{q}}\\ \mathbb{q}\aleph_{\emptyset\Theta}\end{Bmatrix}dV,$$

$$\begin{Bmatrix}\mathbb{P}_{\Theta\mathbb{q}}\\ \mathbb{P}_{\emptyset\mathbb{q}}\\ \mathbb{P}_{\emptyset\Theta}\end{Bmatrix}=\int_V\begin{Bmatrix}\mathbb{q}^2\aleph_{\Theta\mathbb{q}}\\ \mathbb{q}^2\aleph_{\emptyset\mathbb{q}}\\ \mathbb{q}^2\aleph_{\emptyset\Theta}\end{Bmatrix}dV$$

$$\begin{Bmatrix}\mathbb{Q}_{\Theta\mathbb{q}}\\ \mathbb{Q}_{\emptyset\mathbb{q}}\\ \mathbb{Q}_{\emptyset\Theta}\end{Bmatrix}=\int_V\begin{Bmatrix}\mathbb{q}^3\aleph_{\Theta\mathbb{q}}\\ \mathbb{q}^3\aleph_{\emptyset\mathbb{q}}\\ \mathbb{q}^3\aleph_{\emptyset\Theta}\end{Bmatrix}dV,$$

$$\begin{Bmatrix}\mathbb{R}_{\Theta\mathbb{q}}\\ \mathbb{R}_{\emptyset\mathbb{q}}\\ \mathbb{R}_{\emptyset\Theta}\end{Bmatrix}=\int_V\begin{Bmatrix}\mathbb{q}^4\aleph_{\Theta\mathbb{q}}\\ \mathbb{q}^4\aleph_{\emptyset\mathbb{q}}\\ \mathbb{q}^4\aleph_{\emptyset\Theta}\end{Bmatrix}dV$$

$$\begin{Bmatrix}\mathbb{S}_{\Theta\mathbb{q}}\\ \mathbb{S}_{\emptyset\mathbb{q}}\\ \mathbb{S}_{\emptyset\Theta}\end{Bmatrix}=\int_V\begin{Bmatrix}\mathbb{q}^5\aleph_{\Theta\mathbb{q}}\\ \mathbb{q}^5\aleph_{\emptyset\mathbb{q}}\\ \mathbb{q}^5\aleph_{\emptyset\Theta}\end{Bmatrix}dV$$

$$\{\mathfrak{M}_0,\mathfrak{M}_1,\mathfrak{M}_2,\mathfrak{M}_3,\mathfrak{M}_4,\mathfrak{M}_5,\mathfrak{M}_6\}=\int_V(\{1,\mathbb{q},\mathbb{q}^2,\mathbb{q}^3,\mathbb{q}^4,\mathbb{q}^5,\mathbb{q}^6\}\rho)\mathrm{r}^2\sin(\emptyset)d\Theta dzd\emptyset \tag{17}$$

3. Solution methodology

The Harmonic Differential Quadrature Method (HDQM) (Fazaeli *et al*. 2016, Habibi *et al*. 2017, 2019a, c, Safarpour *et al*. 2018, 2019b, 2020, Alipour *et al*. 2020, Ebrahimi *et al*. 2020, Ghazanfari *et al*. 2020, Chen *et al*. 2022) is a numerical technique designed for the efficient and accurate solution of differential equations, particularly those arising in structural mechanics and vibration analysis. Unlike traditional differential quadrature methods that rely on polynomial approximations, HDQM employs harmonic functions, such as trigonometric functions, as basis functions. This choice is particularly advantageous when dealing with problems exhibiting periodic or oscillatory behavior, as harmonic functions naturally capture these characteristics. The method discretizes the solution domain into a set of grid points, and the derivatives of the unknown function at these points are approximated as weighted sums of the function values at other grid points. The key to HDQM's efficiency lies in the determination of these weight coefficients, which are derived from the properties of the chosen harmonic basis functions. By leveraging the orthogonality and periodicity of these functions, HDQM can achieve high accuracy with relatively few grid points, leading to reduced computational cost compared to other numerical methods like the finite element method. Furthermore, HDQM is particularly well-suited for problems with complex geometries and boundary conditions, as it can handle non-uniform grid distributions and incorporate various types of boundary conditions effectively. The method's ability to accurately approximate derivatives, even at high orders, makes it a powerful tool for solving eigenvalue problems, nonlinear differential equations, and dynamic analysis problems, providing a balance between accuracy, efficiency, and versatility. For

the purpose of demonstrating the approximation procedure within the harmonic differential quadrature method (HDQM) using a one-dimensional function, the subsequent relation defines the p-th derivative of $\mathcal{F}(\emptyset)$ in terms of $\emptyset$:

$$\frac{\partial^p \mathcal{F}(\emptyset)}{\partial \emptyset^p} = \sum_{j=1}^{N} \mathcal{G}_{ij}^{(p)} \mathcal{F}(\emptyset) \quad \mathcal{F}or\ i = 1,2,\ldots,N_\emptyset\ and\ p = 1,2,\ldots,N_\emptyset - 1 \tag{18}$$

In this context, $N_\emptyset$ signifies the total count of discrete grid points employed within the solution domain. The symbol $\mathcal{G}_{ij}^{(p)}$ represents the weight coefficients, with *j* ranging from 1 to $N_\emptyset$, associated with the *i*th grid point in the solution domain. To calculate the weight coefficients for first-order derivatives, $\mathcal{G}_{ij}^{(1)}$, when *i* is not equal to *j*, the following relation is used:

$$\mathcal{G}_{\mathrm{ij}}^{(1)} = \frac{\pi \mathrm{P}(\emptyset_i)}{2\mathrm{P}(\emptyset_j)\sin\left[(\emptyset_i - \emptyset_j)/2\pi\right]}, \mathrm{i,j=1,2,...,N}_\emptyset \tag{19}$$

here

$$P(\emptyset_i) = -\sum_{\mathrm{j=1,j}\neq i}^{N_\emptyset} \sin\left(\frac{\pi(\emptyset_i - \emptyset_j)}{2}\right),\ \text{for j=1,2,3,...,N}_\emptyset \tag{20}$$

To determine the weight coefficients for the first-order derivatives, $\mathcal{G}_{ij}^{(1)}$, in the case where i equals j, the following relation is used:

$$\mathcal{G}_{\mathrm{ii}}^{(1)} = -\sum_{\mathrm{j=1,j}\neq i}^{N_\emptyset} \mathcal{G}_{\mathrm{ij}}^{(1)},\ \text{for i=1,2,3,...,N}_\emptyset \tag{21}$$

For the determination of the weight coefficients for the second-order derivatives, $\mathcal{G}_{ij}^{(2)}$, when $i \neq j$, the following relation is employed:

$$\mathcal{G}_{\mathrm{ij}}^{(2)} = \mathcal{G}_{\mathrm{ij}}^{(1)}\left(2\mathcal{G}_{\mathrm{ij}}^{(1)} - \pi\cot\left(\frac{\emptyset_i - \emptyset_j}{2} \times \pi\right)\right), \mathrm{i,j=1,2,3,...,N}_\emptyset \tag{22}$$

For the determination of the weight coefficients (Dai *et al*. 2023b, Gu *et al*. 2023, Li *et al*. 2023, Lu *et al*. 2023a, b, Ma *et al*. 2023, Peng *et al*. 2023, Sabzevari *et al*. 2023, Shariati *et al*. 2023, Tang *et al*. 2023, Wang *et al*. 2023b, Yang *et al*. 2023, Zhang *et al*. 2023a, b, c, 2024a, d, Zhao *et al*. 2023, Zheng *et al*. 2023, Guo *et al*. 2024, Liang *et al*. 2024, Song *et al*. 2024, Xiao *et al*. 2024, Yin *et al*. 2024, Yu *et al*. 2024, Zisong and Habibi 2024) for the second-order derivatives, $\mathcal{G}_{ij}^{(2)}$, when $i = j$, the following relation is employed:

$$\mathcal{G}_{\mathrm{ii}}^{(2)} = -\sum_{\mathrm{j=1,j}\neq i}^{N_r} \mathcal{G}_{\mathrm{ij}}^{(2)},\ \text{for i=1,2,3,...,N}_\emptyset \tag{23}$$

The Chebyshev–Gauss–Lobatto grid distribution was chosen for its desirable convergence properties. The Chebyshev–Gauss–Lobatto (CGL) grid distribution is a powerful and widely utilized technique in numerical analysis, particularly within spectral methods and differential quadrature methods, for its exceptional convergence properties and ability to minimize Runge's phenomenon. Unlike uniform grid distributions, which can lead to oscillations and instability, especially when approximating high-order polynomials or functions with sharp gradients, the CGL grid strategically places nodes according to the roots of Chebyshev polynomials. This distribution concentrates grid points near the boundaries of the domain, where higher resolution is often required to accurately capture boundary layers or rapid changes in function behavior. Specifically, the CGL grid points are defined as the extrema of the *n*-th order Chebyshev polynomial, effectively clustering nodes at the endpoints of the interval [-1, 1] and gradually spacing them out towards the center. This non-uniform distribution not only enhances accuracy but also improves the stability of numerical solutions, particularly for problems involving oscillatory solutions or high-frequency components. Furthermore, the CGL grid's inherent connection to orthogonal polynomials facilitates efficient computation of derivatives and integrals, making it a valuable tool for solving differential equations and performing spectral analysis. In essence, the Chebyshev–Gauss–Lobatto grid distribution offers a robust and accurate approach to discretizing continuous domains, enabling the efficient and reliable solution of complex numerical problems across various scientific and engineering disciplines. The coordinates of the grid points, $(\emptyset_i, \Theta_j)$, on the reference surface are then computed using the following equation:

$$\emptyset_i = \emptyset_0 + \frac{\emptyset}{2}\left(1 - \cos\left(\frac{(i-1)}{(N_\emptyset - 1)}\pi\right)\right) \quad i = 1,2,3,\ldots,N_\emptyset \tag{24}$$

$$\Theta_j = \Theta_0 + \frac{\Theta}{2}\left(1 - \cos\left(\frac{(j-1)}{(N_\Theta - 1)}\pi\right)\right) \quad j = 1,2,3,\ldots,N_\Theta \tag{25}$$

The displacement field expressions are given as below,

$$\begin{aligned}
&\mathfrak{R}_0(\emptyset,\Theta,\mathfrak{Y}) = a_0(\emptyset,\Theta)\exp(i\mathcal{L}\mathfrak{Y}), && \mathfrak{S}_0(\emptyset,\Theta,\mathfrak{Y}) = \mathscr{b}_0(\emptyset,\Theta)\exp(i\mathcal{L}\mathfrak{Y}),\\
&\mathfrak{T}_0(\emptyset,\Theta,\mathfrak{Y}) = c_0(\emptyset,\Theta)\exp(i\mathcal{L}\mathfrak{Y}), && \mathfrak{R}_1(\emptyset,\Theta,\mathfrak{Y}) = a_1(\emptyset,\Theta)\exp(i\mathcal{L}\mathfrak{Y}),\\
&\mathfrak{S}_1(\emptyset,\Theta,\mathfrak{Y}) = \mathscr{b}_1(\emptyset,\Theta)\exp(i\mathcal{L}\mathfrak{Y}), && \mathfrak{T}_1(\emptyset,\Theta,\mathfrak{Y}) = c_1(\emptyset,\Theta)\exp(i\mathcal{L}\mathfrak{Y}),\\
&\mathfrak{R}_2(\emptyset,\Theta,\mathfrak{Y}) = a_2(\emptyset,\Theta)\exp(i\mathcal{L}\mathfrak{Y}), && \mathfrak{S}_2(\emptyset,\Theta,\mathfrak{Y}) = \mathscr{b}_2(\emptyset,\Theta)\exp(i\mathcal{L}\mathfrak{Y}),\\
&\mathfrak{T}_2(\emptyset,\Theta,\mathfrak{Y}) = c_2(\emptyset,\Theta)\exp(i\mathcal{L}\mathfrak{Y}), && \mathfrak{R}_3(\emptyset,\Theta,\mathfrak{Y}) = a_3(\emptyset,\Theta)\exp(i\mathcal{L}\mathfrak{Y}),\\
&\mathfrak{S}_3(\emptyset,\Theta,\mathfrak{Y}) = \mathscr{b}_3(\emptyset,\Theta)\exp(i\mathcal{L}\mathfrak{Y}), && \mathfrak{T}_3(\emptyset,\Theta,\mathfrak{Y}) = c_3(\emptyset,\Theta)\exp(i\mathcal{L}\mathfrak{Y}),\\
&\mathfrak{R}_4(\emptyset,\Theta,\mathfrak{Y}) = a_4(\emptyset,\Theta)\exp(i\mathcal{L}\mathfrak{Y}), && \mathfrak{S}_4(\emptyset,\Theta,\mathfrak{Y}) = \mathscr{b}_4(\emptyset,\Theta)\exp(i\mathcal{L}\mathfrak{Y}),\\
&\mathfrak{T}_4(\emptyset,\Theta,\mathfrak{Y}) = && \mathfrak{R}_5(\emptyset,\Theta,\mathfrak{Y}) =
\end{aligned} \tag{26}$$

$$c_4(\emptyset,\Theta)\exp(i\mathcal{L}\mathcal{Y}), \qquad a_5(\emptyset,\Theta)\exp(i\mathcal{L}\mathcal{Y}),$$

$$\mathfrak{S}_5(\emptyset,\Theta,\mathcal{Y}) = \mathfrak{b}_5(\emptyset,\Theta)\exp(i\mathcal{L}\mathcal{Y}), \qquad \mathfrak{T}_5(\emptyset,\Theta,\mathcal{Y}) = c_5(\emptyset,\Theta)\exp(i\mathcal{L}\mathcal{Y}).$$

Substitution of Eqs. (15), (18), and (26) into Eqs. (16a-r)

$$\left\{\begin{bmatrix}[\mathcal{M}_{dd}] & [\mathcal{M}_{db}]\\ [\mathcal{M}_{bd}] & [\mathcal{M}_{bb}]\end{bmatrix}\mathcal{L}^2+\begin{bmatrix}[\mathcal{K}_{dd}] & [\mathcal{K}_{db}]\\ [\mathcal{K}_{bd}] & [\mathcal{K}_{bb}]\end{bmatrix}\right\}\begin{Bmatrix}\Xi_d\\ \Xi_b\end{Bmatrix}=0 \qquad (27)$$

By solving Eq. (27), the natural frequency of the system can be achieved.

4. Numerical results and discussion

4.1 Materiel properties

Table 1 details the material properties for the constituent components of the volleyball ball, including the graphene oxide powder (GOP) reinforcement and the epoxy (resin) matrix, as well as the composite ball itself. These values are adopted from Reference (Zhang *et al*. 2020).

4.2 Validation

The new material and method presented in the current study need to be verified by comparing to the results of other studies in the similar structure and loading conditions. In this regard, the problem of vibrational behavior evaluation from Liu *et al*. (2021a). The results are presented for two different parameter variation namely the mode number of vibration and the GOP distribution patterns. It is seen that the current method provides similar results to the selected reference which validate our methodology. On the other hand, different variation in pattern of GOP results in different natural frequency of the volleyball shell structure which will be discussed in next sections in details along with several other parameters.

4.3 Parametric study

In this segment, we delve into the intricate relationship between various parameters and configurations within the nanocomposite shell of the volleyball, focusing on their influence on the structure's natural frequency. Fig. 2 presents a comparative study of layer count effects across different GOP configurations. For the GOP-X configuration, a clear correlation emerges: increasing the number of layers initially produces a substantial rise in natural frequency. However, this effect plateaus at higher layer counts, indicating a diminishing return on additional layering. This observation suggests that the GOP-X configuration's dynamic stiffness is primarily influenced by the initial layering, with subsequent additions providing marginal improvements. In stark contrast, the GOP-O configuration displays an inverse relationship, highlighting the sensitivity of this configuration to layer count variations. Interestingly, the uniform GOP distribution proves to be immune to changes in layer count, maintaining a consistent natural frequency. This comparative analysis reveals the critical interplay between GOP distribution and layer count in determining the dynamic response of the nanocomposite shell.

Table 1 The properties of GOPs, polymer, and ball

Polymer epoxy (matrix)	ball	GOPs
$v_m = 0.42$	$m_b\ (gr) = 260$	$v_{GOP} = 0.165$
$\mathcal{E}_m\ (Mpa) = 25$	$\emptyset_{\mathrm{i}} = 10\ [deg]$	$\rho_{GOP}\ (\frac{kg}{m^3}) = 1090$
	$\emptyset_o = 170\ [deg]$	$\mathcal{E}_{GOP}\ (Gpa) = 444.8$
		$d_{GOP}(nm) = 500$
		$h_{GOP}(nm) = 0.95$

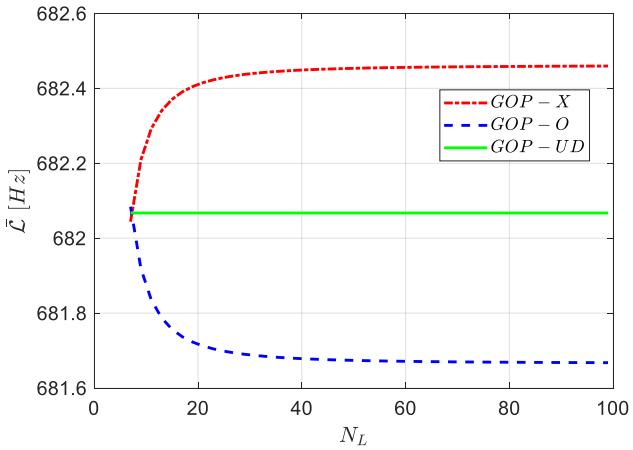

Fig. 2 Effect of GOP-distribution pattern and number of layers on the natural frequency of volleyball ball

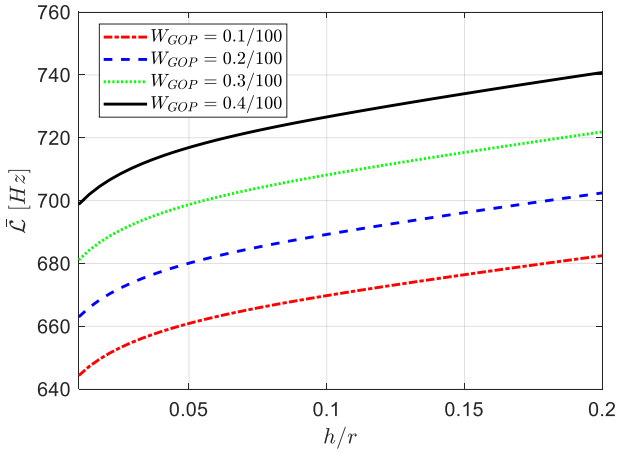

Fig. 3 Effect of h/r aspect ratio and W_{GOP} on the natural frequency of volleyball ball

Fig. 3 presents the parametric analysis of the nano-composite shell's fundamental natural frequency as a function of the thickness-to-radius ratio, denoted as h/R, and the weight fraction of graphene oxide powders (GOPs), denoted as w. The results indicate a monotonic increase in the natural frequency with increasing h/R across all considered GOP weight fractions. This behavior is attributed to the direct relationship between the shell's stiffness matrix and its thickness. Furthermore, the introduction of GOPs, characterized by their high Young's modulus, leads to an increase in the composite's effective

Table 2 Frequency parameter of the composite spherical shell

Mode number	Epoxy		GPL-UD		GPL-X		GPL-O	
	Ref. (Liu *et al*. 2021a)	Present	Ref. (Liu *et al*. 2021a)	Present	Ref. (Liu *et al*. 2021a)	Present	Ref. (Liu *et al*. 2021a)	Present
1	19.2432	19.2361	40.0892	40.0045	29.6019	29.5891	43.7133	43.6901
2	1.1613	1.1601	2.4194	2.4012	2.4203	2.4117	2.4196	2.4032
3	1.8362	1.8351	3.8253	3.8212	3.8263	3.8215	3.8251	3.8182
4	2.4635	2.4602	5.1322	5.1310	5.1324	5.1301	5.1309	5.1292

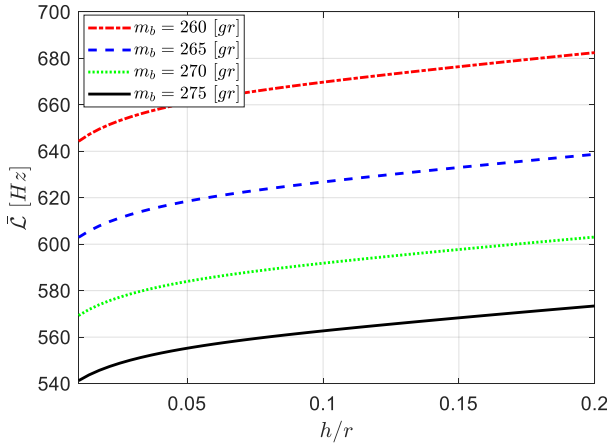

Fig. 4 Effect of total mass of the ball m_b and h/r on the natural frequency of volleyball ball

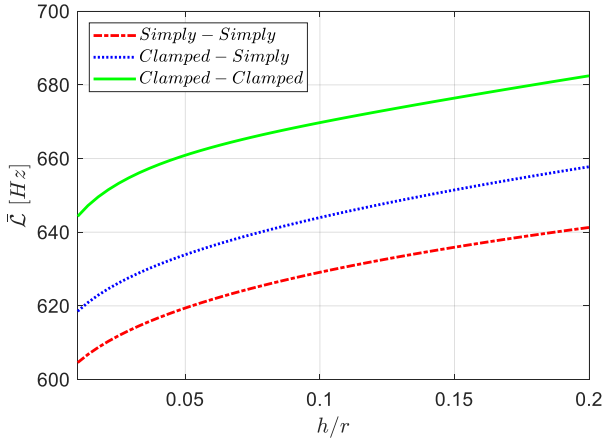

Fig. 6 Effect of boundary condition and h/r on the natural frequency of volleyball ball

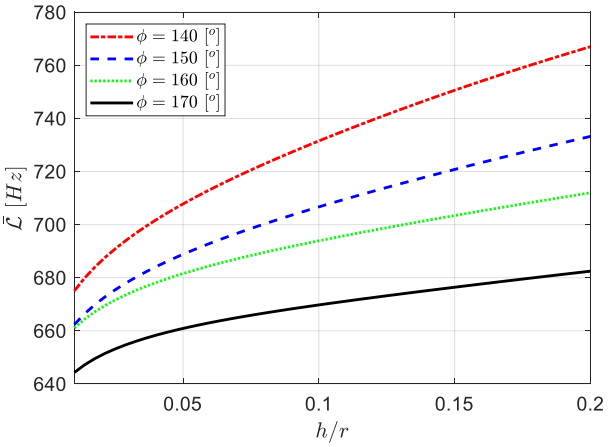

Fig. 5 Effect of angle ϕ and h/r on the natural frequency of volleyball ball

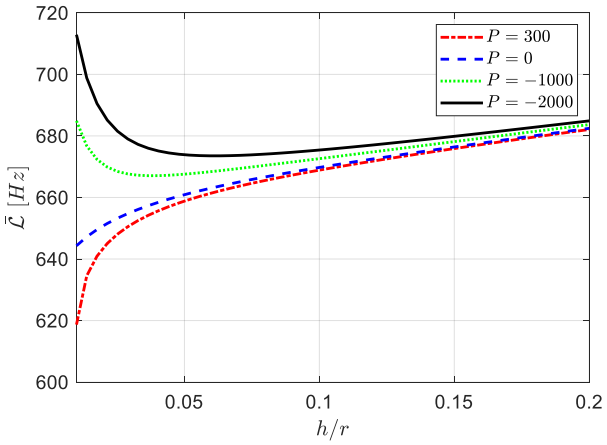

Fig. 7 Effect of parameter P and h/r on the natural frequency of volleyball ball

modulus, thereby elevating the natural frequency. The data suggests a synergistic effect of both geometric and material parameters on the dynamic characteristics of the shell.

The dynamic response of the spherical shell model, specifically the natural frequency, is shown to be dependent on the total mass (m) of the volleyball, as illustrated in Fig. 4 for varying thicknesses (h). An increase in mass, maintaining constant geometric parameters, results in a decrease in material density, consequently leading to a reduction in the natural frequency. This behavior is consistent with the inverse proportionality between mass/ density and natural frequency within dynamic systems. Furthermore, the effect of the thickness-to-radius aspect ratio (h/R) on the natural frequency, as depicted in Fig. 4, demonstrates a trend analogous to that observed in Fig. 3, reinforcing the influence of geometric parameters on the system's dynamic characteristics.

Increase in angle ϕ in general decreases the natural frequency of the structure for all thickness values as seen in Fig. 5. However, the degree of increase is different ϕs is based on the thickness and the value of the angle ϕ. In low angles, the gradient of increase in the natural frequency is higher than other angle values.

The state of boundary condition could be determinative in calculating the natural frequency of the structure as demonstrated in Fig. 6. In this Figure, change in the boundary condition alters the state of natural frequency in

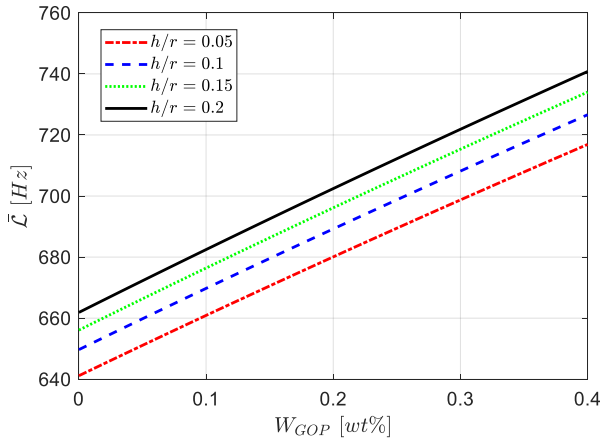

Fig. 8 Effect of W_{GOP} and h/r on the natural frequency of volleyball ball

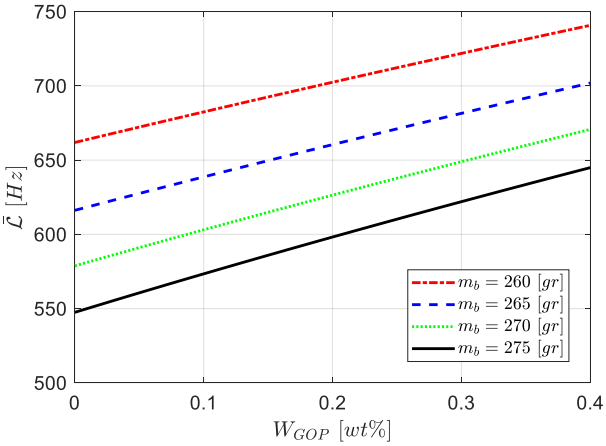

Fig. 9 Effect of total mass of the ball m_b and W_{GOP} on the natural frequency of volleyball ball

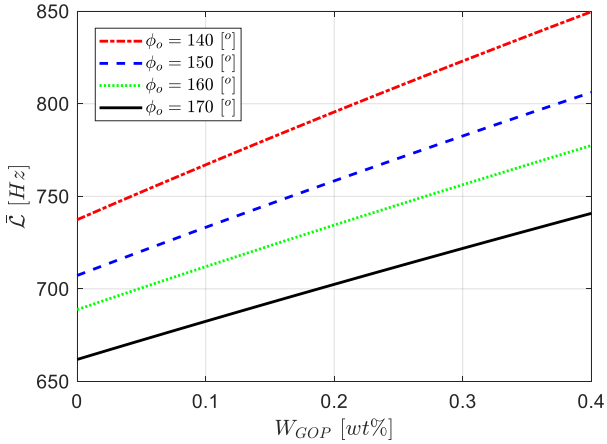

Fig. 10 Effect of angle ϕ_0 and W_{GOP} on the natural frequency of volleyball ball

different values of h/r. The simply supported boundary condition has the smallest natural frequency among other boundary conditions for a constant value of thickness to radius ratio. In addition, highest frequency values correspond to the clamped boundary condition.

In all above parametric studies it was assumed that the internal pressure of the ball in equal to ambient pressure. However. In reality the pressure inside the ball is positive. Variation in internal pressure of the ball changes the natural frequency value of the structure as shown in Fig. 7. In is seen that change in parameter P from positive values to negative values considerably alters the behavior of frequency curves. In positive and zero values of parameter P, the natural frequency increase monotonically for all values of h/r. However, in negative values the behavior of the natural frequency changes as in low values of the h/r the natural frequancy decreases as h/r increases. In each parameter P there could be seen a turning point in the curves in which the natural frequency begins to rise. All the curves converges and coincides at high value of thickness to radius ratio.

Simultaneous effects of h/r aspect ratio and weight fraction of GOP are depicted in Fig. 8. Similar to Fig. 3, increase in both of these parameters results in increase in the natural frequency of the structure. However, one important feature of the present graph is the semi-linear change in the natural frequency due to change in the weight fraction of the GOP which could not be deduced from Fig. 3.

The linear rise of natural frequency as a result of increase in weight fraction of GOP is also observed in Fig. 9 for different values of ball mass m_b. Higher ball masses results in lower values of natural frequency as seen in this Figure.

Simultaneous effects of angle ϕ and weight fraction of GOP are depicted in Fig. 10. Similar to Fig. 3, increase in W_{GOP} parameter results in increase in the natural frequency of the structure. However, one important feature of the present graph is decrease in the natural frequency of the structure with increase in angle ϕ_0 from 140° to 170°.

5. Discussion

The observations of the natural frequency in engineering materials and spherical structures could not be easily generalized to balls in sport. One important feature of ball mechanics in a game in the large deformation they endure in contrast to the small deformations in the other structures. On the other hand, effect of internal pressure is disregarded in most calculations where it has an influential role in determining vibration and other mechanical properties of the balls. One another differences between ball and other engineering structures are the loading condition and state of t boundary conditions. The loading in the balls are mostly in the form impact loading and there are no detectable boundary conditions in a free ball. Therefore, in the analyses, some tricks have to be adopted to apply boundary conditions in mechanical analyses of the balls in sports. Zhang and Yu (2012) experimentally examined the condition of buckling in ping-pong balls using both quasi-static and impact loading conditions. The state of buckling as well as the mode shape of buckling during several tests were measured and simulated. The numerical simulations were similar to the experimental results in the condition of incorporating viscoelasticity properties of the ball. The dynamic buckling condition of sport balls with different materials and thicknesses were examined by Cross (Cross 2014). In another experimental examination of buckling

condition in the ping-pong balls, Rémond *et al*. (2022) found that initiation of buckling occurs when deflection of the shell exceeds twice the thickness of the ball in both quasi-static and dynamic loadings. Moreover, they found that the most energy dissipation in the ball impact is due to friction energy loss. Asai *et al*. (2007) considered instability of ball in the air due to aerodynamic forces. They observed some phenomena in the air flow around soccer ball which were different from other balls with smooth and non-smooth surface conditions. Therefore, it is important that the ball sport to be investigated in their own context to find about their mechanical behavior and also to aid designers to design balls that less affect the performance of individual players.

Furthermore, the inherent material anisotropy and heterogeneity present in sports balls, particularly those constructed from layered nanocomposites, introduce complexities not typically encountered in traditional engineering structures. The fabrication processes, often involving molding and bonding, can lead to variations in material properties across the ball's surface and through its thickness. This non-uniformity significantly impacts the ball's dynamic response, particularly under impact loading. Unlike homogeneous engineering materials, where properties are assumed to be consistent, sports balls exhibit a gradient of stiffness and damping characteristics. This gradient influences the propagation of stress waves and the resulting vibrational modes, making accurate prediction challenging. Therefore, advanced computational models, such as those incorporating finite element analysis with detailed material characterization, are essential to capture these nuances and provide a more realistic representation of ball behavior. Additionally, the viscoelastic nature of the materials used in sports balls, which is often temperature-dependent, further complicates the analysis. These factors must be considered to accurately predict the performance of a sports ball under varying environmental and playing conditions.

Moreover, the interaction between the ball and the playing surface or the player's hand introduces further complexities that are often overlooked in conventional engineering analyses. The coefficient of restitution, which dictates the energy loss during impact, is highly dependent on the surface properties of both the ball and the contact surface. Surface roughness, material compliance, and impact velocity all play crucial roles in determining the rebound characteristics. For example, the spin imparted on a ball during impact significantly alters its trajectory due to the Magnus effect, a phenomenon that is highly sensitive to the ball's surface texture and aerodynamic properties. Additionally, the human factor, including the variability in hand-ball contact and the subjective perception of ball feel, adds another layer of complexity. The tactile feedback perceived by the player is influenced by the ball's surface texture, stiffness, and damping characteristics, which in turn affects their performance. Consequently, the development of sports balls requires a multidisciplinary approach that integrates material science, biomechanics, and fluid dynamics, as well as considering the player's sensory experience. This holistic approach ensures that the design of sports balls not only optimizes performance but also enhances the player's comfort and control.

6. Conclusions

In this study, we successfully modeled and analyzed the vibrational response of a graphene oxide-reinforced volleyball subjected to impact loading. By employing Hamilton's principle and spherical shell coordinates, we derived and solved the governing equations using the generalized differential quadrature (GDQ) method and analytical approaches. Our analysis revealed a critical relationship between the ball's radius and its dynamic stability, demonstrating that variations in radius significantly alter vibrational characteristics. Furthermore, we established that increased ball mass, independent of size, enhances stability upon ground impact, indicating improved resistance to deformation and vibration. These findings provide a quantitative framework for optimizing volleyball design by elucidating the complex interplay between material reinforcement, geometry, and impact dynamics. Ultimately, this research facilitates the development of volleyballs with superior stability and performance. The main results of this work are:

- Higher ball masses results in lower values of natural frequency.
- Variation in internal pressure of the ball changes the natural frequency value of the structure
- Increase in the thickness of ball shell causes increase in the natural frequency of the structure

The natural frequency rises linearly as a result of increase in weight fraction of GO P

References

Al-Furjan, M.S.H., Bolandi, S.Y., Habibi, M., Ebrahimi, F., Chen, G. and Safarpour, H. (2021a), "Enhancing vibration performance of a spinning smart nanocomposite reinforced microstructure conveying fluid flow", *Eng. Comput*., 1-16. https://doi.org/10.1007/s00366-020-01255-w

Al-Furjan, M.S.H., Habibi, M., Ebrahimi, F., Mohammadi, K. and Safarpour, H. (2020a), "Wave dispersion characteristics of high-speed-rotating laminated nanocomposite cylindrical shells based on four continuum mechanics theories", *Waves Random Complex Med*., 1-27. https://doi.org/10.1080/17455030.2020.1831099

Al-Furjan, M.S.H., Habibi, M., Jung, D.W., Chen, G., Safarpour, M. and Safarpour, H. (2021b), "Chaotic responses and nonlinear dynamics of the graphene nanoplatelets reinforced doubly-curved panel", *Eur. J. Mech. A Solids*, **85**, 104091. https://doi.org/10.1016/j.euromechsol.2020.104091

Al-Furjan, M.S.H., Habibi, M., Ni, J., Jung, D.w. and Tounsi, A. (2020b), "Frequency simulation of viscoelastic multi-phase reinforced fully symmetric systems", *Eng. Comput*., **38**(Suppl 5), 3725-3741. https://doi.org/10.1007/s00366-020-01200-x

Al-Furjan, M.S.H., Oyarhossein, M.A., Habibi, M., Safarpour, H. and Jung, D.W. (2022), "Wave propagation simulation in an electrically open shell reinforced with multi-phase nano-composites", *Eng. Comput*., **38**(1), 629-645. https://doi.org/10.1007/s00366-020-01167-9

Alam, M., Guo, Y., Bai, Y. and Luo, S. (2025), "Post-critical nonlinear vibration of nonlocal strain gradient beam involving surface energy effects", *J. Sound Vib*., **601**, 118930. https://doi.org/10.1016/j.jsv.2025.118930

Alipour, M., Torabi, M.A., Sareban, M., Lashini, H., Sadeghi, E., Fazaeli, A., Habibi, M. and Hashemi, R. (2020), "Finite element

and experimental method for analyzing the effects of martensite morphologies on the formability of DP steels", *Mech. Based Des. Struct.*, **48**(5), 525-541. https://doi.org/10.1080/15397734.2019.1633343

Allam, O., Draiche, K., Bousahla, A.A., Bourada, F., Tounsi, A., Benrahou, K.H., Mahmoud, S., Bedia, E.A. and Tounsi, A. (2020), "A generalized 4-unknown refined theory for bending and free vibration analysis of laminated composite and sandwich plates and shells", *Comput. Concr.*, **26**(2), 185-201. http://doi.org/10.12989/cac.2020.26.2.185

Amelirad, O. and Assempour, A. (2019), "Experimental and crystal plasticity evaluation of grain size effect on formability of austenitic stainless steel sheets", *J. Manuf. Proc.*, **47**, 310-323. https://doi.org/10.1016/j.jmapro.2019.09.035

Amelirad, O. and Assempour, A. (2021), "Coupled continuum damage mechanics and crystal plasticity model and its application in damage evolution in polycrystalline aggregates", *Eng. Comput.*, 1-15. https://doi.org/10.1007/s00366-021-01346-2

Arshid, E., Khorasani, M., Soleimani-Javid, Z., Amir, S. and Tounsi, A. (2021), "Porosity-dependent vibration analysis of FG microplates embedded by polymeric nanocomposite patches considering hygrothermal effect via an innovative plate theory", *Eng. Comput.*, 1-22. https://doi.org/10.1007/s00366-021-01382-y

Asai, T., Seo, K., Kobayashi, O. and Sakashita, R. (2007), "Fundamental aerodynamics of the soccer ball", *Sports Eng.*, **10**(2), 101-109. https://doi.org/10.1007/BF02844207

Bakoura, A., Bourada, F., Bousahla, A.A., Tounsi, A., Benrahou, K.H., Tounsi, A., Al-Zahrani, M.M. and Mahmoud, S. (2021), "Buckling analysis of functionally graded plates using HSDT in conjunction with the stress function method", *Comput. Concr.*, **27**(1), 73-83. http://doi.org/10.12989/cac.2021.27.1.073

Bekkaye, T.H.L., Fahsi, B., Bousahla, A.A., Bourada, F., Tounsi, A., Benrahou, K.H., Tounsi, A. and Al-Zahrani, M.M. (2020), "Porosity-dependent mechanical behaviors of FG plate using refined trigonometric shear deformation theory", *Comput. Concr.*, **26**(5), 439-450. http://doi.org/10.12989/cac.2020.26.5.439

Bellal, M., Hebali, H., Heireche, H., Bousahla, A.A., Tounsi, A., Bourada, F., Mahmoud, S., Bedia, E. and Tounsi, A. (2020), "Buckling behavior of a single-layered graphene sheet resting on viscoelastic medium via nonlocal four-unknown integral model", *Steel Compos. Struct.*, **34**(5), 643-655. https://doi.org/10.12989/scs.2020.34.5.643

Bendenia, N., Zidour, M., Bousahla, A.A., Bourada, F., Tounsi, A., Benrahou, K.H., Bedia, E.A., Mahmoud, S. and Tounsi, A. (2020), "Deflections, stresses and free vibration studies of FG-CNT reinforced sandwich plates resting on Pasternak elastic foundation", *Comput. Concr.*, **26**(3), 213-226. http://doi.org/10.12989/cac.2020.26.3.213

Chen, F., Chen, J., Duan, R., Habibi, M. and Khadimallah, M.A. (2022), "Investigation on dynamic stability and aeroelastic characteristics of composite curved pipes with any yawed angle", *Compos. Struct.*, 115195. https://doi.org/10.1016/j.compstruct.2022.115195

Cross, R. (2014), "Impact behavior of hollow balls", *Am. J. Phys.*, **82**(3), 189-195. https://doi.org/10.1119/1.4839055

Dai, Z., Tang, H., Wu, S., Habibi, M., Moradi, Z. and Ali, H.E. (2023a), "Nonlinear consecutive dynamic instabilities of thermally shocked composite circular plates on the softening elastic foundation", *Thin Wall. Struct.*, **186**, 110645. https://doi.org/10.1016/j.tws.2023.110645

Dai, Z., Wu, S., Habibi, M. and Ali, H.E. (2023b), "Application of point interpolation mesh-free method for magneto/electro rheological vibrations of sandwich conical panels", *Aerosp. Sci. Technol.*, 108180. https://doi.org/10.1016/j.ast.2023.108180

Ebrahimi, F. and Barati, M.R. (2016), "Analytical solution for nonlocal buckling characteristics of higher-order inhomogeneous nanosize beams embedded in elastic medium", *Adv. Nano Res.*, **4**(3), 229-249. https://doi.org/10.12989/anr.2016.4.3.229

Ebrahimi, F., Habibi, M. and Safarpour, H. (2019a), "On modeling of wave propagation in a thermally affected GNP-reinforced imperfect nanocomposite shell", *Eng. Comput.*, **35**(4), 1375-1389. https://doi.org/10.1007/s00366-018-0669-4

Ebrahimi, F., Hajilak, Z.E., Habibi, M. and Safarpour, H. (2019b), "Buckling and vibration characteristics of a carbon nanotube-reinforced spinning cantilever cylindrical 3D shell conveying viscous fluid flow and carrying spring-mass systems under various temperature distributions", *Proceedings of the Institution of Mechanical Engineers, Part C: Journal of Mechanical Engineering Science*, **233**(13), 4590-4605. https://doi.org/10.1177/0954406219832323

Ebrahimi, F., Hashemabadi, D., Habibi, M. and Safarpour, H. (2020), "Thermal buckling and forced vibration characteristics of a porous GNP reinforced nanocomposite cylindrical shell", *Microsyst. Technol.*, **26**(2), 461-473. https://doi.org/10.1007/s00542-019-04542-9

Esmailpoor Hajilak, Z., Pourghader, J., Hashemabadi, D., Sharifi Bagh, F., Habibi, M. and Safarpour, H. (2019), "Multilayer GPLRC composite cylindrical nanoshell using modified strain gradient theory", *Mech. Based Des. Struct.*, **47**(5), 521-545. https://doi.org//10.1080/15397734.2019.1566743

Fazaeli, A., Habibi, M. and Ekrami, A.a. (2016), "Experimental and finite element comparison of mechanical properties and formability of dual phase steel and ferrite - pearlite steel with the same chemical composition", *Metall. Eng.*, **19**(2), 84-93. http://doi.org/10.22076/me.2017.41458.1064

Ge, J., Hong, Y., Zeng, R., Li, Y. and Habibi, M. (2023), "Increasing the attractiveness of physical education training with the involvement of nanotechnology", *Adv. Concr. Constr.*, **16**(6), 291-302. https://doi.org/10.12989/acc.2023.16.6.291

Ghabussi, A., Ashrafi, N., Shavalipour, A., Hosseinpour, A., Habibi, M., Moayedi, H., Babaei, B. and Safarpour, H. (2021), "Free vibration analysis of an electro-elastic GPLRC cylindrical shell surrounded by viscoelastic foundation using modified length-couple stress parameter", *Mech. Based Des. Struct.*, **49**(5), 738-762. https://doi.org/10.1080/15397734.2019.1705166

Ghabussi, A., Habibi, M., NoormohammadiArani, O., Shavalipour, A., Moayedi, H. and Safarpour, H. (2020), "Frequency characteristics of a viscoelastic graphene nanoplatelet–reinforced composite circular microplate", *J. Vib. Control*, **27**(1-2), 101-118. https://doi.org/10.1177/1077546320923930

Ghazanfari, A., Soleimani, S.S., Keshavarzzadeh, M., Habibi, M., Assempuor, A. and Hashemi, R. (2020), "Prediction of FLD for sheet metal by considering through-thickness shear stresses", *Mech. Based Des. Struct.*, **48**(6), 755-772. https://doi.org/10.1080/15397734.2019.1662310

Gu, X., He, J., Wang, Z., Li, M., Habibi, M. and Hashemabadi, D. (2023), "Application of hyperbolic differential quadrature method for vibration responses of the electrorheological disk", *Eng. Anal. Bound. Elem.*, **155**, 599-615. https://doi.org/10.1016/j.enganabound.2023.05.035

Guo, Y., Maalla, A. and Habibi, M. (2024), "Electroelastic wave dispersion in the rotary piezoelectric NEMS sensors/actuators via nonlocal strain gradient theory", *Mech. Syst. Signal Pr.*, **216**, 111453. https://doi.org/10.1016/j.ymssp.2024.111453

Habibi, M., Darabi, R., Sa, J.C.D. and Reis, A. (2021a), "An innovation in finite element simulation via crystal plasticity assessment of grain morphology effect on sheet metal formability", *Proceedings of the Institution of Mechanical Engineers, Part L: Journal of Materials: Design and Applications*, **235**(8), 1937-1951.

https://doi.org/10.1177/14644207211024686
Habibi, M., Ghazanfari, A., Assempour, A., Naghdabadi, R. and Hashemi, R. (2017), "Determination of forming limit diagram using two modified finite element models", *Mech. Eng*., **48**(4), 141-144. https://doi.org/10.22060/MEJ.2016.664
Habibi, M., Habibi, M., Toghroli, E., Safa, M. and Shariati, M. (2024), "Frequency responses of a graphene oxide reinforced concrete structure", *Eídos*, **17**(24), 63-79. https://doi.org/10.29019/eidos.v17i24.1382
Habibi, M., Hashemabadi, D. and Safarpour, H. (2019a), "Vibration analysis of a high-speed rotating GPLRC nano-structure coupled with a piezoelectric actuator", *Eur. Phys. J. Plus*, **134**(6), 307. https://doi.org/10.1140/epjp/i2019-12742-7
Habibi, M., Hashemi, R., Ghazanfari, A., Naghdabadi, R. and Assempour, A. (2018a), "Forming limit diagrams by including the M–K model in finite element simulation considering the effect of bending", *Proceedings of the Institution of Mechanical Engineers, Part L: Journal of Materials: Design and Applications*, **232**(8), 625-636.
Habibi, M., Hashemi, R., Sadeghi, E., Fazaeli, A., Ghazanfari, A. and Lashini, H. (2016), "Enhancing the mechanical properties and formability of low carbon steel with dual-phase micro-structures", *J. Mater. Eng. Perform*., **25**(2), 382-389.
Habibi, M., Hashemi, R., Tafti, M.F. and Assempour, A. (2018b), "Experimental investigation of mechanical properties, formability and forming limit diagrams for tailor-welded blanks produced by friction stir welding", *J. Manuf. Proc*., **31**, 310-323. https://doi.org/10.1016/j.jmapro.2017.11.009
Habibi, M., Mohammadgholiha, M. and Safarpour, H. (2019b), "Wave propagation characteristics of the electrically GNP-reinforced nanocomposite cylindrical shell", *J. Brazil. Soc. Mech. Sci. Eng*., **41**(5), 221. | https://doi.org/10.1007/s40430-019-1715-x
Habibi, M., Mohammadi, A., Safarpour, H. and Ghadiri, M. (2019c), "Effect of porosity on buckling and vibrational characteristics of the imperfect GPLRC composite nanoshell", *Mech. Based Des. Struct*., **49**(6), 1-30. https://doi.org/10.1080/15397734.2019.1701490
Habibi, M., Mohammadi, A., Safarpour, H. and Ghadiri, M. (2021b), "Effect of porosity on buckling and vibrational characteristics of the imperfect GPLRC composite nanoshell", *Mech. Based Des. Struct*., **49**(6), 811-840. https://doi.org/10.1080/15397734.2019.1701490
Habibi, M., Mohammadi, A., Safarpour, H., Shavalipour, A. and Ghadiri, M. (2019d), "Wave propagation analysis of the laminated cylindrical nanoshell coupled with a piezoelectric actuator", *Mech. Based Des. Struct*., 1-19. https://doi.org/10.1080/15397734.2019.1697932
Habibi, M., Taghdir, A. and Safarpour, H. (2019e), "Stability analysis of an electrically cylindrical nanoshell reinforced with graphene nanoplatelets", *Compos. Part B Eng*., **175**, 107125. https://doi.org/10.1016/j.compositesb.2019.107125
Hachemi, H., Bousahla, A.A., Kaci, A., Bourada, F., Tounsi, A., Benrahou, K.H., Tounsi, A., Al-Zahrani, M.M. and Mahmoud, S. (2021), "Bending analysis of functionally graded plates using a new refined quasi-3D shear deformation theory and the concept of the neutral surface position", *Steel Compos. Struct*., **39**(1), 51-64. http://doi.org/10.12989/scs.2021.39.1.051
Hadji, L. and Avcar, M. (2021), "Nonlocal free vibration analysis of porous FG nanobeams using hyperbolic shear deformation beam theory", *Adv. Nano Res.*, **10**(3), 281-293. https://doi.org/10.12989/anr.2021.10.3.281
He, L., Habibi, M. and Khorami, M. (2024), "Semi-analytical stability behavior of composite concrete structures via modified non-classical theories", *Adv. Concr. Constr*., **17**(4), 187. https://doi.org/10.12989/acc.2024.17.4.187
Heidari, F., Taheri, K., Sheybani, M., Janghorban, M. and Tounsi, A. (2021), "On the mechanics of nanocomposites reinforced by wavy/defected/aggregated nanotubes", *Steel Compos. Struct*., **38**(5), 533-545. https://doi.org/10.12989/scs.2021.38.5.533
Huang, J., Pan, Z., Yang, S., Habibi, M. and Safa, M. (2024), "Bending-based solution methodology using eigenvalue-eigenvector approach for analysis of foldable reinforced Golf Clubs cylindrical shell", *Mech. Adv. Mater. Struct*., 1-14. https://doi.org/10.1080/15376494.2024.2378372
Huang, Y., Karami, B., Shahsavari, D. and Tounsi, A. (2021), "Static stability analysis of carbon nanotube reinforced polymeric composite doubly curved micro-shell panels", *Arch. Civil Mech. Eng*., **21**(4), 1-15. https://doi.org/10.1007/s43452-021-00291-7
Hutchinson, J.W. (2016), "Buckling of spherical shells revisited", *Proceedings of the Royal Society A: Mathematical, Physical and Engineering Sciences*, **472**(2195), 20160577. https://doi.org/10.1098/rspa.2016.0577
Jin, Z., Huo, W., Habibi, M. and Albaijan, I. (2024), "Thermo-foldable bending analysis of tunable shells using a higher-order modeling", *Mech. Adv. Mater. Struct*., 1-14. https://doi.org/10.1080/15376494.2024.2369263
Karami, B., Janghorban, M. and Tounsi, A. (2019), "Galerkin's approach for buckling analysis of functionally graded anisotropic nanoplates/different boundary conditions", *Eng. Comput*., **35**(4), 1297-1316. https://doi.org/10.1007/s00366-018-0664-9
Kumar, Y., Gupta, A. and Tounsi, A. (2021), "Size-dependent vibration response of porous graded nanostructure with FEM and nonlocal continuum model", *Adv. Nano Res*., **11**(1), 1-17. https://doi.org/10.12989/anr.2021.11.1.001
Li, J., Tang, F. and Habibi, M. (2020), "Bi-directional thermal buckling and resonance frequency characteristics of a GNP-reinforced composite nanostructure", *Eng. Comput*., 1-22. https://doi.org/10.1007/s00366-020-01110-y
Li, J., Wu, Z., Habibi, M. and Albaijan, I. (2024), "An inspection of the metal-foam beam considering torsional dynamic responses", *Solid State Commun*., **391**, 115638. https://doi.org/10.1016/j.ssc.2024.115638
Li, X., Li, M., Habibi, M., Najaafi, N. and Safarpour, H. (2023), "Optimization of hybrid energy management system based on high-energy solid-state lithium batteries and reversible fuel cells", *Energy*, **283**, 128454. https://doi.org/10.1016/j.energy.2023.128454
Liang, Z., Zhao, Y., Yu, H., Habibi, M. and Mahmoudi, T. (2024). "Artificial neural networks coupled with numerical approach for the stability prediction of non-uniform functionally graded microscale cylindrical structures", *Structures*, **60**, 105826. https://doi.org/10.1016/j.istruc.2023.105826
Liu, D., Zhou, Y. and Zhu, J. (2021a), "On the free vibration and bending analysis of functionally graded nanocomposite spherical shells reinforced with graphene nanoplatelets: Three-dimensional elasticity solutions", *Eng. Struct*., **226**, 111376. https://doi.org/10.1016/j.engstruct.2020.111376
Liu, H., Shen, S., Oslub, K., Habibi, M. and Safarpour, H. (2021b), "Amplitude motion and frequency simulation of a composite viscoelastic microsystem within modified couple stress elasticity", *Eng. Comput*., 1-15. https://doi.org/10.1007/s00366-021-01316-8
Lori, E.S., Ebrahimi, F., Supeni, E.E.B., Habibi, M. and Safarpour, H. (2020), "Frequency characteristics of a GPL-reinforced composite microdisk coupled with a piezoelectric layer", *Eur. Phys. J. Plus*, **135**(2), 144. https://doi.org/10.1140/epjp/s13360-020-00217-x
Lu, L., Liao, K., Habibi, M., Safarpour, H. and Ali, H.E. (2023a). "Numerical methods to predict aero thermally induced vibrations of a curved pipe structure reinforced by GPLs", *Structures*, **55**, 1607-1621.

https://doi.org/10.1016/j.istruc.2023.06.10

Lu, S., Li, S., Habibi, M. and Safarpour, H. (2023b), "Improving the thermo-electro-mechanical responses of MEMS resonant accelerometers via a novel multi-layer perceptron neural network", *Measurement*, 113168. https://doi.org/10.1016/j.measurement.2023.113168

Ma, B., Chen, K.Y., Habibi, M. and Albaijan, I. (2023), "Static/dynamic analyses of sandwich micro-plate based on modified strain gradient theory", *Mech. Adv. Mater. Struct.*, 1-8. https://doi.org/10.1080/15376494.2023.2219453

Man, Y., Habibi, M. and Maleki, B. (2024), "Biodiesel synthesis from waste coconut scum oil utilizing SnFe2O4/cigarette butt-derived biochar as a magnetic nanocatalyst: Optimization, kinetic and thermodynamic study", *Chem. Eng. Res. Des.*, **210**, 311-327. https://doi.org/10.1016/j.cherd.2024.08.033

Matouk, H., Bousahla, A.A., Heireche, H., Bourada, F., Bedia, E., Tounsi, A., Mahmoud, S., Tounsi, A. and Benrahou, K. (2020), "Investigation on hygro-thermal vibration of P-FG and symmetric S-FG nanobeam using integral Timoshenko beam theory", *Adv. Nano Res.*, **8**(4), 293-305. https://doi.org/10.12989/anr.2020.8.4.293

Menasria, A., Kaci, A., Bousahla, A.A., Bourada, F., Tounsi, A., Benrahou, K.H., Tounsi, A., Bedia, E.A. and Mahmoud, S. (2020), "A four-unknown refined plate theory for dynamic analysis of FG-sandwich plates under various boundary conditions", *Steel Compos. Struct.*, **36**(3), 355-367. http://doi.org/10.12989/scs.2020.36.3.355

Moayedi, H., Habibi, M., Safarpour, H., Safarpour, M. and Foong, L.K. (2019), "Buckling and frequency responses of a graphene nanoplatelet reinforced composite microdisk", *Int. J. Appl. Mech.*, **11**(10), 1950102. https://doi.org/10.1142/S1758825119501023

Peng, S., Habibi, M. and Pourjabari, A. (2023), "Generalized differential quadrature element solution, swarm, and GA optimization technique to obtain the optimum frequency of the laminated rotary nanostructure", *Eng. Anal. Bound. Elem.*, **151**, 101-114. https://doi.org/10.1016/j.enganabound.2023.02.052

Pourjabari, A., Hajilak, Z.E., Mohammadi, A., Habibi, M. and Safarpour, H. (2019), "Effect of porosity on free and forced vibration characteristics of the GPL reinforcement composite nanostructures", *Comput. Math. Appl.*, **77**(10), 2608-2626.

Rémond, T., Dolique, V., Vittoz, F., Antony, S., Rinaldi, R.G., Manin, L. and Géminard, J.C. (2022), "Dynamical buckling of a table-tennis ball impinging normally on a rigid target: Experimental and numerical studies", *Phys. Rev. E*, **106**(1), 014207. https://doi.org/10.1103/PhysRevE.106.014207

Sabzevari, F., Amelirad, O., Moradi, Z. and Habibi, M. (2023), "Artificial intelligence evaluation of COVID-19 restrictions and speech therapy effects on the autistic children's behavior", *Sci. Rep.*, **13**(1), 4312. https://doi.org/10.1038/s41598-022-25902-y

Safarpour, H., Ghanizadeh, S.A. and Habibi, M. (2018), "Wave propagation characteristics of a cylindrical laminated composite nanoshell in thermal environment based on the nonlocal strain gradient theory", *Eur. Phys. J. Plus*, **133**(12), 532. https://doi.org/10.1140/epjp/i2018-12385-2

Safarpour, H., Hajilak, Z.E. and Habibi, M. (2019a), "A size-dependent exact theory for thermal buckling, free and forced vibration analysis of temperature dependent FG multilayer GPLRC composite nanostructures restring on elastic foundation", *Int. J. Mech. Mater. Des.*, **15**(3), 569-583. https://doi.org/10.1007/s10999-018-9431-8

Safarpour, H., Pourghader, J. and Habibi, M. (2019b), "Influence of spring-mass systems on frequency behavior and critical voltage of a high-speed rotating cantilever cylindrical three-dimensional shell coupled with piezoelectric actuator", *J. Vib. Control*, **25**(9), 1543-1557. https://doi.org/10.1177/1077546319828465

Safarpour, M., Ebrahimi, F., Habibi, M. and Safarpour, H. (2020), "On the nonlinear dynamics of a multi-scale hybrid nano-composite disk", *Eng. Comput.*, 1-20. https://doi.org/10.1007/s00366-020-00949-5

Safarpour, M., Ebrahimi, F., Habibi, M. and Safarpour, H. (2021), "On the nonlinear dynamics of a multi-scale hybrid nano-composite disk", *Eng. Comput.*, **37**(3), 2369-2388. https://doi.org/10.1007/s00366-020-00949-5

Shamsaddini Lori, E., Ebrahimi, F., Elianddy Bin Supeni, E., Habibi, M. and Safarpour, H. (2021), "The critical voltage of a GPL-reinforced composite microdisk covered with piezoelectric layer", *Eng. Comput.*, **37**(4), 3489-3508. https://doi.org/10.1007/s00366-020-01004-z

Shariati, A., Habibi, M., Tounsi, A., Safarpour, H. and Safa, M. (2021), "Application of exact continuum size-dependent theory for stability and frequency analysis of a curved cantilevered microtubule by considering viscoelastic properties", *Eng. Comput.*, **37**(4), 3629-3648. https://doi.org/10.1007/s00366-020-01024-9

Shariati, M., Kamyab, H., Habibi, M., Ahmadi, S., Naghipour, M., Gorjinezhad, F., Mohammadirad, S. and Aminian, A. (2023), "Sulfuric acid resistance of concrete containing coal waste as a partial substitute for fine and coarse aggregates", *Fuel*, **348**, 128311. https://doi.org/10.1016/j.fuel.2023.128311

Shi, X., Li, J. and Habibi, M. (2020), "On the statics and dynamics of an electro-thermo-mechanically porous GPLRC nanoshell conveying fluid flow", *Mech. Based Des. Struct.*, 1-37. https://doi.org/10.1080/15397734.2020.1772088

Soleimani-Javid, Z., Arshid, E., Khorasani, M., Amir, S. and Tounsi, A. (2021), "Size-dependent flexoelectricity-based vibration characteristics of honeycomb sandwich plates with various boundary conditions", *Adv. Nano Res.*, **10**(5), 449-460. http://doi.org/10.12989/anr.2021.10.5.449

Song, G., Zou, Y., Nie, Y., Habibi, M., Albaijan, I. and Toghroli, E. (2024), "Application of Hashin–Shtrikman bounds homogenization model for frequency analysis of imperfect FG bio-composite plates", *J. Mech. Behav. Biomed. Mater.*, **151**, 106321. https://doi.org/10.1016/j.jmbbm.2023.106321

Tahir, S.I., Tounsi, A., Chikh, A., Al-Osta, M.A., Al-Dulaijan, S.U. and Al-Zahrani, M.M. (2021), "An integral four-variable hyperbolic HSDT for the wave propagation investigation of a ceramic-metal FGM plate with various porosity distributions resting on a viscoelastic foundation", *Waves Random Complex Med.*, 1-24. https://doi.org/10.1080/17455030.2021.1942310

Tang, J., Wu, S., Habibi, M., Safarpour, M. and Ali, H.E. (2023), "Flutter analysis of multi-directional functionally graded sector poroelastic disks", *Aerosp. Sci. Technol.*, **140**, 108481. https://doi.org/10.1016/j.ast.2023.108481

Van Vinh, P. and Tounsi, A. (2021), "The role of spatial variation of the nonlocal parameter on the free vibration of functionally graded sandwich nanoplates", *Eng. Comput.*, 1-19. https://doi.org/10.1007/s00366-021-01475-8

Wang, S., He, J., Fan, J., Sun, P. and Wang, D. (2023a), "A time-domain method for free vibration responses of an equivalent viscous damped system based on a complex damping model", *J. Low Freq. Noise Vib. Active Control*, **42**(3), 1531-1540. https://doi.org/10.1177/14613484231157514

Wang, Y., Jia, Q., Deng, T., Habibi, M., Al-Kikani, S. and Ali, H.E. (2023b), "Wave propagation analysis of the ball in the handball's game", *Struct. Eng. Mech.*, **85**(6), 729-742. https://doi.org/10.12989/sem.2023.85.6.729

Wang, L., Habibi, M. and Huang, G. (2024a), "Smart analysis of sandwich foldable cylinders as gymnastic accessories", *Mech. Adv. Mater. Struct.*, 1-18. https://doi.org/10.1080/15376494.2024.2411414

Wang, W., Zhang, J., Habibi, M. and Albaijan, I. (2024b), "Stretchable-thickness model for dynamic responses of

graphene origami reinforced badminton sport plate", *Mech. Adv. Mater. Struct.*, 1-13. https://doi.org/10.1080/15376494.2024.2373976

Wang, Y. and Sigmund, O. (2023), "Multi-material topology optimization for maximizing structural stability under thermo-mechanical loading", *Comput. Meth. Appl. Mech. Eng.*, **407**, 115938. https://doi.org/10.1016/j.cma.2023.115938

Xiang, J., Lai, Y., Moradi, Z. and Khorami, M. (2023), "Wave propagation phenomenon of functionally graded graphene oxide powder-strengthened nanocomposite curved beam", *Solid State Commun.*, 115193. https://doi.org/10.1016/j.ssc.2023.115193

Xiao, H., Habibi, M. and Habibi, M. (2024), "Bulk wave propagation analysis of imperfect FG bio-composite beams resting on variable elastic medium", *Mater. Today Commun.*, **39**, 108524. https://doi.org/10.1016/j.mtcomm.2024.108524

Xu, W., Pan, G., Moradi, Z. and Shafiei, N. (2021), "Nonlinear forced vibration analysis of functionally graded non-uniform cylindrical microbeams applying the semi-analytical solution", *Compos. Struct.*, **275**, 114395. https://doi.org/10.1016/j.compstruct.2021.11439

Yang, C., Su, C., Hu, H., Habibi, M., Safarpour, H. and Khadimallah, M.A. (2023), "Performance optimization of photovoltaic and solar cells via a hybrid and efficient chimp algorithm", *Solar Energy*, **253**, 343-359. https://doi.org/10.1016/j.solener.2023.02.036

Yang, Q., Zeng, X., Guo, K., Cao, S., Wei, K., Shan, W. and Tamura, Y. (2025), "Analysis of vortex-induced vibration in flexible risers using a physically-meaningful wake-oscillator model", *Eng. Struct.*, **325**, 119415. https://doi.org/10.1016/j.engstruct.2024.119415

Yin, J., Zou, Y., Li, J., Zhang, W., Li, X. and Habibi, M. (2024), "Dynamic stability and frequency responses of the tilted curved nanopipes in a supersonic airflow via 2D hybrid nonlocal strain gradient theory", *Eng. Struct.*, **301**, 117240. https://doi.org/10.1016/j.engstruct.2023.117240

Yu, C., Lin, P., Wu, Z., Habibi, M. and Zhang, W. (2024), "Multi-load effect on the deformation analysis of composite nano reinforced origami sandwich panel", *Mech. Adv. Mater. Struct.*, 1-19. https://doi.org/10.1080/15376494.2024.2367015

Zerrouki, R., Karas, A., Zidour, M., Bousahla, A.A., Tounsi, A., Bourada, F., Tounsi, A., Benrahou, K.H. and Mahmoud, S. (2021a), "Effect of nonlinear FG-CNT distribution on mechanical properties of functionally graded nano-composite beam", *Struct. Eng. Mech.*, **78**(2), 117-124. https://doi.org/10.12989/sem.2021.78.2.117

Zhang, D., Huang, X., Wang, T., Habibi, M., Albaijan, I. and Toghroli, E. (2024a), "Dynamic stability improvement in spinning FG-piezo cylindrical structure using PSO-ANN and firefly optimization algorithm", *Mater. Sci. Eng. B*, **302**, 117210. https://doi.org/10.1016/j.mseb.2024.117210

Zhang, H., Habibi, M. and Zou, Y. (2024b), "Static analysis of foldable pressurized and thermally loaded cylindrical shell as an expander in sport equipment reinforced by G-Ori nanofillers", *Mech. Adv. Mater. Struct.*, 1-13. https://doi.org/10.1080/15376494.2024.2412307

Zhang, Q., Xie, M., Zhou, D., Habibi, M. and Khorami, M. (2024c), "Bending responses of graphene nanoplatelets reinforced sandwich cylindrical micro panel with piezoelectric layers", *Mech. Adv. Mater. Struct.*, 1-16. https://doi.org/10.1080/15376494.2024.2385008

Zhang, Q., Zou, X., Wang, Y. and Habibi, M. (2023a), "Study on photocatalytic, electric, and sensing behavior of Co-and Ag-codoped tin dioxide (SnO2) nano particles", *Mater. Sci. Eng. B*, **296**, 116687. https://doi.org/10.1016/j.mseb.2023.116687

Zhang, S., Lai, Y., Chen, K., Habibi, M., Khorami, M. and Haider Mussa, Z. (2023b), "Influence of MWCNT's waviness and aggregation factors on wave dispersion response of MWCNT-strengthened nanocomposite curved beam", *Structures*, **53**, 1239-1249. https://doi.org/10.1016/j.istruc.2023.04.024

Zhang, X., Li, J., Cui, Y., Habibi, M., Ali, H.E., Albaijan, I. and Mahmoudi, T. (2023c), "Static analysis of 2D-FG nonlocal porous tube using gradient strain theory and based on the first and higher-order beam theory", *Steel Compos. Struct.*, **49**(3), 293-306. https://doi.org/10.12989/scs.2023.49.3.293

Zhang, X.W. and Yu, T.X. (2012), "Experimental and numerical study on the dynamic buckling of ping-pong balls under impact loading", *Int. J. Nonlinear Sci. Numer. Simul.*, **13**(1), 81-92. https://doi.org/10.1515/ijnsns-2011-103

Zhang, Y., Wang, Z., Tazeddinova, D., Ebrahimi, F., Habibi, M. and Safarpour, H. (2021), "Enhancing active vibration control performances in a smart rotary sandwich thick nanostructure conveying viscous fluid flow by a PD controller", *Waves Random Complex Med.*, 1-24. https://doi.org/10.1080/17455030.2021.1948627

Zhang, Z., Li, Y., Wu, H., Zhang, H., Wu, H., Jiang, S. and Chai, G. (2020), "Mechanical analysis of functionally graded graphene oxide-reinforced composite beams based on the first-order shear deformation theory", *Mech. Adv. Mater. Struct.*, **27**(1), 3-11. https://doi.org/10.1080/15376494.2018.1444216

Zhao, H., Li, C., Fu, Y., Oyarhossein, M.A., Habibi, M. and Safarpour, H. (2023), "Quasi-static indentation, low-velocity impact, and resonance responses of the laminated double-curved panel considering various boundary conditions", *Thin Wall. Struct.*, **183**, 110360. https://doi.org/10.1016/j.tws.2022.110360

Zhao, J., Wan, L., Habibi, M. and Brahmia, A. (2024), "An adaptive neuro-fuzzy approach using IoT data in predicting springback in ultra-thin stainless steel sheets with consideration of grain size", *Adv. Nano Res.*, **17**(2), 109. https://doi.org/10.12989/.2024.17.2.109

Zheng, W., Liu, J., Oyarhossein, M.A., Safarpour, H. and Habibi, M. (2023), "Prediction of nth-order derivatives for vibration responses of a sandwich shell composed of a magneto-rheological core and composite face layers", *Eng. Anal. Bound. Elem.*, **146**, 170-183. https://doi.org/10.1016/j.enganabound.2022.10.019

Zhu, L., Ren, H., Habibi, M., Mohammed, K.J. and Khadimallah, M.A. (2022), "Predicting the environmental economic dispatch problem for reducing waste nonrenewable materials via an innovative constraint multi-objective Chimp Optimization Algorithm", *J. Clean. Prod.*, 132697. https://doi.org/10.1016/j.jclepro.2022.132697

Zisong, Z. and Habibi, M. (2024), "AI-assisted prediction of St14 steel sheets formability: Neural-fuzzy systems and crystal plasticity assessments", *Structures*, **65**, 106633

CC